Lehigh University
Lehigh Preserve

Theses and Dissertations

2000

Quantifying elemental compositions in heterogeneous materials using a new imaging SIMS method

William A. Lamberti
Lehigh University

Follow this and additional works at: http://preserve.lehigh.edu/etd

Recommended Citation
Lamberti, William A., "Quantifying elemental compositions in heterogeneous materials using a new imaging SIMS method" (2000). *Theses and Dissertations.* Paper 642.

This Thesis is brought to you for free and open access by Lehigh Preserve. It has been accepted for inclusion in Theses and Dissertations by an authorized administrator of Lehigh Preserve. For more information, please contact preserve@lehigh.edu.

Lamberti, William A.

Quantifying Elemental Compositions in Heterogeneous Materials Using a New Imaging...

June 2000

Quantifying Elemental Compositions in Heterogeneous Materials Using A New Imaging SIMS Method

by

William A. Lamberti

A Thesis

Presented to the Graduate and Research Committee

of Lehigh University

in Candidacy for the Degree of

Master of Engineering

in Materials Science and Engineering

Lehigh University

Spring 2000

<u>Certificate of Approval</u>

This thesis is accepted and approved in partial fulfillment of the requirements for the Master of Engineering.

May 5, 2000

Date

Thesis Advisor

Co-Advisor

Department Chairperson

Acknowledgements

This work is first and foremost dedicated to Caroline, Billy, and Joey.

They have been far too patient.

Many thanks for the support and encouragement given by C.E. Lyman, whose excitement in science rekindled my spirit.

To D. Leta & B. Horn who remind me how much fun SIMS is.

To M. Disko, for his friendship and guidance.

To J. Koo, R. Bangaru, & R. Mueller for an education in metallurgy.

Finally, thanks to Mom & Dad, who showed me the way.

Table of Contents

Chapter	Contents	Page
I	SIMS Quantification in Heterogeneous Materials - Light Element Segregation in Steels	3
II	The General SIMS Method	6
III	SIMS Quantification Methods	11
	A. Existing Methods	
	1) Relative sensitivity factors	11
	2) Ion implanted internal standards	12
	3) Matrix ion species ratios	14
	4) CsM^+ cluster ion detection	16
	5) Infinite velocity method	17
	B. Imaging internal reference method	18
IV	Requirements for Quantitative SIMS Image Acquisition	21
	A. Ion Image conversion and detection	21
	B. Detector resolution	22
	C. Detector efficiency	23
	D. Detector dynamic range	23
	E. Detector linearity	24
	F. Detector frame rate	24
V	Image Detectors Selected	25
	A. Video intensified cooled CCD camera	25
	B. Resistive anode encoder ("RAE")	25
VI	Determination of trace boron in model steel alloys	28
	A. Experimental	28
	B. Results	31
	C. Discussion	33
VII	Conclusion	37
	Appendix A	39
	Appendix B	52

Table of Contents
(cont.)

Appendix C.. 62
References.. 64
Figures
Tables
Vita

List of Figures

Figure	Description
1	SIMS sputter process.
2	SIMS instrument schematic (Cameca 3f).
3	SIMS positive ion images of commercial reactor lining.
4	Channel plate structure as viewed in SEM - cross section.
5	Channel plate structure - input surface.
6	Schematic of Resistive Anode Encoder.
7	RAE detector sensor.
8	B-Fe phase diagram.
9	Two Alloys side by side in SIMS sample mount.
10	Boron images for both alloys, side by side.
11	Typical line profile across both 8ppm & 12ppm steels .
12	Second linescan showing resolved precipitates on 12 ppm steel alone.
13	Plot of 12ppm/8ppm B/Fe ion ratios vs. position.
14	Boron concentration profile obtained by SIMS.
15	Secondary electron image of original P20 phosphor.
16	Impact of camera resolution on detected image data content.
17	Efficiency curves for typical CCD's.
18	Response curve for video system.
19	VICCD camera, manual controller, software control panel, and schematic.
20	ITI MV150/40 image processor system layout.
21	Reference waveform and waveform monitor trace.
22	Reference waveform as digitized by the SunVideo grabber.
23	Reference waveform as digitized by original Crystal image processor.
24	Reference waveform as digitized by ITI MV 150/40.
25	RAE analysis of 12 ppm and 0 ppm samples.
26	Comparison of video and RAE image data results.

List of Tables

Table	Description
1	Summary of major SIMS quantification schemes.
2	Outline of HSLA steels used in this study.
3	Measurement conditions used for imaging analysis.
4	Summary of boron relative quantification results.
5	Ideal spatial oversampling requirements at each stage of image conversion.
6	Actual spatial sampling at each stage of image conversion for the original Cameca 3f design.
7(a)	Spatial sampling at each stage of image conversion in improved design for this study.
7(b)	Calculated intrinsic digitized SIMS image resolution as a function of camera pixel resolution.
8	Estimation of net detector chain efficiency.
9	VICCD camera components and specifications.

ABSTRACT

Presented here is a unique method utilizing imaging dynamic Secondary Ion Mass Spectrometry ("SIMS") for quantifying elemental compositions in heterogeneous samples. This technique, described as an "imaging internal reference" ("IIR") method is applied specifically to the quantitative detection of solid-solution boron levels in High Strength Low Alloy ("HSLA") steel plates, both with and without boron precipitation present. Model HSLA steel plates employed for this study contained varying amounts of trace boron, estimated to range between 1 - 10 ppm (based upon melt formula composition). These alloys are intended to be used for relative studies of boron composition, as no traceable solid-solution boron standard exists for microanalysis at these concentrations.

This method relies on the imaging capabilities of SIMS, whereby an unknown is mounted with a known reference material in the same field of view, enabling simultaneous imaging of both samples. After obtaining a statistically valid sampling, one then utilizes image processing methods for the post-analysis of the heterogeneous image data. Phases which are not of interest can be excluded, thus enabling the determination of solid-solution concentrations alone. In contrast to all other SIMS quantification schemes, this image-based approach enables heterogeneous samples to be analyzed reliably. Initial studies indicate that excellent results (estimated at +/- 5 %, relative) can be obtained at trace levels (1-12 ppm) in these heterogeneous model alloys.

In acquiring the image data for quantitative analysis, it is critical that the image acquisition chain be treated strictly as a detector system in itself, with proper hardware choices and calibration procedures followed. A detailed examination of the image detection chain shows that the direct ion image data can suffer significant resolution losses in the image conversion process. A discussion of how to best choose the optimal image hardware and acquisition methods will also be provided.

I. SIMS Quantification in Heterogeneous Materials - Light Element Segregation in Steels

A reliable method based upon imaging Secondary Ion Mass Spectrometry for the quantification of trace species in heterogeneous materials promises to provide a significant advantage in understanding the micro-chemistry and phase behavior of commercially important systems. The method developed in this work requires careful attention to the process of image detection, acquisition, and subsequent image processing. These initial studies involving model steel alloys indicate that this image-based approach does provide the ability to perform excellent relative quantification.

Continuous casting methods are employed routinely in commercial steel manufacturing facilities. As the melt cools, the possibility exists for macro-segregation to occur due to constitutional supercooling at the solidification front. If present, this macro-segregation ultimately manifests itself within the centerline of the slab as a precipitate-rich zone. Macro-segregation, as opposed to micro-segregation, can not generally be removed by a subsequent homogenizing heat treatment. Preventing the formation of this precipitate-rich zone is therefor critical to avoid impaired material properties such as fracture susceptibility.

High Strength Low Alloy ("HSLA") steels used for this study are low-carbon (0.15 %)[‡] steels with manganese (1.5 %) as a principal alloying agent. Small amounts

---

[‡] Throughout document, all values in weight percent unless otherwise noted.

of other species are frequently added in varying amounts to improve strength and toughness. Examples of these species include titanium (0..02 %), and vanadium or niobium (0.02 % - 0.1 %). Trace levels of light elements such as nitrogen (0.020 %) and boron (0.0005 % - 0.006 %) can also be required to enhance particular properties[†]. Boron is typically added to improve hardenability, especially in steels with less carbon[1]. Monitoring the solid-solution levels of potential precipitate-forming species thus becomes a critical capability in order to prevent macro-segregation in the as-cast slabs. This is a formidable task in the case of light elements such as boron, especially on a micro-scale (1 μm - 100 μm).

Numerous bulk methods, including wet chemical methods, Inductively Coupled Plasma Atomic Emission Spectroscopy ("ICP/AES") and X-ray Fluorescence Spectroscopy ("XRF") are employed regularly to determine the average bulk composition of materials. These techniques, however, cannot readily determine light element composition (below atomic number 8) at trace levels (tens of ppm) on a microscopic scale (~1 μm). For example, XRF can be used to *detect* boron above 500 ppm, but is not recommended for the quantitative measurement of trace boron below 500 ppm[2]. Electron Microprobe techniques utilizing Wavelength Dispersive Spectroscopy can be used to analyze boron on a local scale (1 - 5 um) but quantitative detection is typically limited to concentrations above 1at%.[3]

Secondary Ion Mass Spectrometry provides extreme sensitivity (ppb-ppm) on

[†] Values in parentheses refer to typical composition ranges for common ASTM-specification high strength low alloy steels.

microscopic length scales (resolution = 0.5 μm laterally; 20 - 100 angstroms in depth)†. The detection and mapping of trace boron distributions in HSLA steels is thus possible using SIMS. However, subsequent SIMS quantification poses significant challenges, as the production of the SIMS signal is highly variable and depends greatly on the local sample chemistry at hand. Resolvable boron-rich phases that may be present as boron oxides will possess a much higher ion yield of $^{11}B^+$ (100 - fold higher, after normalizing for concentration) than for interstitial boron metal contained within the iron lattice. The development of an image-based SIMS method to enable the separation of chemically dissimilar phases thus promises to be a powerful tool for quantitatively studying solid-solution elemental concentrations in these model HSLA steels.

In order to better understand the approach developed herein, an introduction to the general SIMS technique and existing methods of SIMS data quantification is in order. It will be seen that these existing methods are inadequate in cases where the sample is not uniform in composition. An overview of the key issues for successful quantitative SIMS image acquisition is also provided.

---

† Emerging SIMS instruments now can provide lateral resolution below 50 nm, while still maintaining extreme (ppm/ppb) sensitivity (non-gallium primary ions employed).

II. The General SIMS Method

Secondary Ion Mass Spectrometry is an ion beam technique whereby an energetic incident beam of primary ions strikes a sample surface and secondary particles are ejected. The ejected particles are neutral atoms, charged ions, molecules, and electrons. Typically a very small fraction are ionized (secondary ion yield < 1%)[4]. The remaining secondary particles are neutral species and electrons. Higher secondary ion yields result in improved sensitivity. For this reason, either oxygen or cesium ions are used as the primary ion species. Gallium is sometimes used as a primary ion beam to provide higher lateral resolution, but suffers from greatly degraded secondary ion yields and thus poor sensitivity (1000-fold reduction of both). A schematic of the process is shown in Figure 1.

"Dynamic" SIMS refers to the case where a high flux of incident primary ions is used for an analysis. Sample material is slowly removed as the sputter process takes place. Thus high elemental signal levels are produced, and the sample composition can readily be followed as a function of depth. Extensive bond breaking occurs on an atomic scale, limiting the amount of molecular information that can be obtained in this mode. Best detection limits for dynamic SIMS are in the low-to-sub ppb range.

"Static" SIMS refers to the case where a very low primary ion flux is used. Static SIMS obtains its name from the fact that the entire analysis takes place on essentially the topmost monolayer. The maximum amount of sputtering that can occur

while still maintaining static conditions corresponds to direct ion bombardment of less than 0.1% of the top monolayer. Thus, essentially no material removal occurs below the top 1 or 2 monolayers. Primary ion bombardment is kept to a minimum so as to limit the amount of molecular fragmentation that occurs in the sputtering process. Rather than direct sputtering as in the dynamic mode, secondary ions are released from the sample surface due to interactions with the disrupted lattice in the vicinity of the primary ion impact. Many more molecular fragments are released in this process versus the direct sputtering process. As a result, static SIMS is a powerful tool for the study of organic species on surfaces, and provides extensive molecular information. Best detection limits for static SIMS are in the low-to-mid ppm range[4].

All studies herein take place in the dynamic SIMS regime. This regime provides the highest signal strength due to the large primary currents employed. Consequently this method provides optimal elemental detection limits.

In the Cameca [†] "F" series of SIMS instruments, two modes of imaging exist:

(1) Ion "microprobe" mode: a raster-based approach utilizing synchronous detection of the individual masses.

(2) Ion "microscope" mode: a stigmatic[5] approach, analogous to that used in conventional light optical microscopy. This mode is also referred to as "direct ion imaging". Here, the primary ion beam acts as a broad-beam illumination source, and electrostatic ion lenses are used to produce an image plane. No rastering occurs in this mode. Only the stigmatic or "microscope" mode of imaging is employed for these

---

[†] Cameca, 103 Boulevard Saint-Denis/BP6, 92403 Courbevoie Cedex/France.

studies. A schematic of a Cameca 3F instrument is shown in Figure 3. The secondary ions are electrostatically captured by an immersion lens which is a few millimeters from the sample region. At this point all masses originally present in the sputtered volume exist in the secondary ion beam with a wide range of ion energies and angular directions. These ions are then accelerated towards the contrast aperture, where angular discrimination occurs. The ions then proceed on to the electrostatic analyzer. After passing through the electrostatic analyzer, the ions are dispersed in energy so that a narrow range of energies can be selected by the use of a set of energy slits. The width of the energy distribution can be controlled by varying the width of these adjustable energy slits. Exiting the energy slits, the secondary ion beam now contains all of the sputtered ion species within a narrow angular and energy range. The magnet then proceeds to filter the ion beam based upon mass to charge ratio ("m/q"). For singly charged ions q=1. For purposes of this discussion, the secondary ion beam at the exit of the magnet is essentially composed of all ions corresponding to one mass, at a single energy. At the exit of the secondary magnet, if needed, mass filtration can be fine-tuned to provide high selectivity (1/10,000 AMU). All elemental species are ready to be detected, with isotope separation readily achieved.

At the detection point, either particle counting (electron multiplier/faraday cup) or direct ion imaging can take place. The microscope mode of imaging is made possible by the presence of electrostatic ion lenses which are located throughout the instrument. These electrostatic, stigmatic ion lenses act on the secondary ion beam to form both image planes and crossover planes along the optical path. The final image

detection point can visualize either an image or a crossover plane as needed by the operator.

An example of video-based SIMS ion image of a refractory material is provided in Figure 4. This heat insulating, oxide material is used as a spray-dried thermal barrier coating within commercial chemical reactor vessels. The general composition of the refractory was a blend of SiO_2, Al_2O_3, and a variety of other additives. Three individual ion images of $^{28}Si^+$, $^{40}Ca^+$, and $^{7}Li^+$ have been overlaid in RGB space to provide a convenient means to visually determine elemental correlations. In each plane, intensity is proportional to concentration for each element individually. Each element's maximum intensity has been set to grey level 255 for purposes of display (8-bits per plane). Thus, elemental ratios between species are not directly obtained from this type of image display, but spatial relationships are valid.

The image provides useful information that would be impossible to obtain using other methods. Lithium, a minor constituent, with atomic number of 3, cannot be detected by most other techniques. Silicon and calcium are major species, present at the several percent level and higher. Thus, trace and major constituents can be analyzed in the same session. Furthermore, in this case a large field of view is imaged (nearly 0.5mm) but the spatial resolution in the data provides valid information below 6 μm laterally. Large fields of view facilitate statistically relevant sampling as compared to extremely localized techniques such as Transmission Electron Microscopy with Electron Energy Loss Spectroscopy ("TEM/EELS")[6]. For the interested reader, a classic reference covering many of the details of SIMS is authored

by Benninghoven et al.[7] We will now move on to a discussion of the current options for SIMS quantification.

III. SIMS Quantification Methods

A. Existing Methods.

The dominant use of SIMS in the world is within the semiconductor industry. As such, much of the work to date has focussed on technique development that would benefit those analysis types. These most often include the quantitative determination of dopant depth distributions in semiconductor devices. Boron implants in silicon are a classic example, with quantitative profiles possible due to the very well-known matrix environments (silicon, gallium arsenide, etc.) that are usually present in the samples encountered in a production environment.

1) Relative Sensitivity Factors ("RSF's"). [4] Relative sensitivity factors are element-specific calibration factors for a given species in a known matrix such as silicon. The relative error of the RSF approach ranges between +/- 10-50%. RSF's are derived using matching standards for the species and matrix of interest. The reliability of the RSF method is limited by several factors, including:

- the quality and certifiability of the standard itself;
- instrumental variations due to ion optical alignment, focus, and sample tilt;
- degree of match in matrix composition between the original reference material and the current sample at hand.

Note that if the nature of the matrix changes, such as inadvertent oxidization or contamination with small amounts of sodium, then the RSF can become quite

inaccurate in use. Luckily, these problems are less frequent in a semiconductor environment, but in other industrial environments where the sample history can be completely unknown, the RSF approach is not practical unless many samples of the same type are expected.

2) Ion-implanted Internal Standard Method.[8] When analyzing semiconductor materials the matrix composition, degree of crystallinity, and crystallographic orientation are often well-defined. Desired dopants are themselves introduced largely via ion-implantation. Thus, it is possible to introduce an additional implant species, such as a minor isotope of the species of interest, to provide some relative means of quantifying the signals obtained during a SIMS analysis. With attention to the issues discussed below, the range of relative error is typically between 5 - 50%.[9]

This method has several merits, including[10]:

- The quality of the results is not dominated by the reproducibility of the SIMS analysis conditions such as beam current, sample tilt, or secondary optical alignment, since both the standard and the unknown are analyzed simultaneously within the same analysis region.
- Any isotope of any element can be implanted into any matrix.
- The incident flux of the implant species can be reliably duplicated from sample to sample.
- Homogeneous implant distributions can be produced on uniform matrices via rastering of the implant beam across the matrix surface.

In contrast to the above advantages, some of the complicating factors[9] include:

- Target matrix sputtering occurs as a result of the implantation process. Thus, unless the reference implant is introduced simultaneously with the implanted species of interest, some modification of the sample will occur. This can be especially troublesome in analyzing ultra-shallow implants (where the dopant profile peaks below 200 nm in depth).
- Implanted reference species backscattering occurs, thus reducing the actual implanted dose of the standard. The effect is most significant where the majority matrix species has a larger atomic mass than the implant species. Lower incident implant energies (less than 50 keV) also enhance this effect.
- Both diffusion and ion channeling can occur, leading to incorrectly distributed reference species. The species of interest within the sample are also prone to diffusion-induced and ion channeling-induced migration when subjected to an incident implant beam. Samples exhibiting multiple phases with different crystal orientations will thus experience widely different implant distributions versus depth. This is a major factor in the analysis of general industrial samples.

- Dose homogeneity is directly limited by the instrumental performance of the ion implanter. Beam purity, beam stability, raster uniformity, and energy stability all affect the final implanted dose concentration.

3) Matrix Ion Species Ratio Method ("MISR").[11] This method utilizes external standards as a means to calibrate an instrument's sensitivity for a given species, in a given matrix. As locally variable amounts of oxygen in the sample matrix are the major cause of variable ion yields ("matrix effect"), the MISR method also calibrates the signals measured, by means of an imposed oxygen bleed, so that the partial pressure of oxygen near the sample surface can be controlled. A calibration curve of at least two matrix signals versus oxygen partial pressure is then obtained for the standard.

In this approach, one monitors the production of two matrix species signals as well as the species of interest. In the case of the ferrous alloy used in the referenced study (by Ganjei, Leta, and Morrison - NBS-662 steel) the authors monitored the ratio $^{112}Fe_2^+/^{54}Fe^+$ as well as the species to be calibrated ($^{52}Cr^+$). The ratio of the *molecular* iron fragment to the *monatomic* fragment is very sensitive to oxygen pressure, and thus provides a means to correlate the Cr^+ sensitivity factor to the local oxygen concentration at the sample surface. The $^{112}Fe_2^+/^{54}Fe^+$ ratio in an "unknown" sample thus is a direct means to determine the appropriate Cr^+ sensitivity factor . Here the "unknown" still must be nominally of the same composition as the standard used as a calibrant. Employing the MISR method, the average relative error seen for a

series of steels, copper alloys, and aluminum alloys was of the order of 10%. The range of relative error observed was between 3% - 50%.

This method, as in the case of depth profiling utilizing either RSF's or internal standards, has been employed to date most extensively in a non-imaging mode. In fact, it is likely that much of the error encountered in the study above was due to sample micro-heterogeneity. The standards employed were only certified on a bulk basis, and were not certified as being homogeneous on a micro-scale. The authors address this concern, and stipulated that indeed, the sample must meet certain criteria for uniformity in order for the method to be valid.

A unique example of the careful application of the RSF and MISR methods using a video-based image acquisition system can be found in the work of Michiels, et al (1990)[12]. This was generally successful in the study presented, with reported relative errors of 16% - 22% as averaged for seven species in an aluminum alloy. Best results were obtained utilizing the MISR method, whereby an attempt was made to convert the ion images into concentration maps on a local basis within each elemental image. The MISR correction included corrections for the presence of precipitates. For the MISR analyses, the *average* relative error for seven species measured was 16.7%. The *range* of error between the certified values and the final calculated values ranged from 0% to 73%. The largest error (73%) occurred with the lowest concentration species, which was titanium, present at a level *300 times higher* than the boron levels in the HSLA steels studied herein. Boron and titanium have almost identical detection limits as positive secondary ions.

4) "Cesium + Matrix" Cluster Ion Detection ("CsM^+"). [13] When using a primary beam of Cs^+, the detection of positive secondary ions that are formed, through combination of the primary Cs-ion with a sputtered neutral atom above the sample surface, provides a signal that is relatively insensitive to most SIMS matrix effects. Since sputtered *neutral* atoms are effectively detected in this method, the ionization yield, and hence the matrix effect, should only have a small effect on the signal levels. Concentration should be the measured variable in a given elemental analysis. Theoretically the CsM^+ molecular signal can be monitored, and with minor calibration for sputter rate, the sample stoichiometry can then be determined.

In fact, the CsM^+ method has been shown to be capable of very good quantification (+/- 10%, relative) of major species in several systems. Without the use of standards, semi-quantitative results (+/- 50%, relative) can be obtained.[13,14]

A drawback is that the method utilizes only lower energy secondary ion clusters, and these signal strengths are orders of magnitude lower than the simple monatomic species. The use of Cs_2M^+ ions (note: Cs *dimers* here) can improve the sensitivity somewhat[15], but this still falls far short of the sensitivity obtained using simple monatomic species by a factor of 10^3 - 10^5. The result is that only major species are candidates for quantification using the CsM^+ method. Imaging of these low energy ions is also very poor, especially in the case of insulators (as compared to the more common oxygen analysis for insulators). Thus, for insulators, relatively poor sensitivity, image resolution, and depth resolution accompany the CsM^+ method.

5) Infinite Velocity Method ("IVM"). [16] This method is treated in some detail in Appendix C. In general the technique relies upon an extrapolation of energy distribution plots for individual species of interest. In theory the approach should eliminate the matrix effect, thus local chemical environment should not have any impact on the ion yield in an analysis taken to the infinite velocity limit.

To utilize this method, measurements of the secondary ion energy distribution for species of interest are converted into "inverse velocity plots". In these plots, the secondary ion intensity is plotted versus the inverse of the ion velocity (which is determined from the measured kinetic energy). [17] These plots are then used as the first step in applying the IVM, with results that are theoretically free of matrix-induced errors.[18] For a detailed treatment of the method, the works referred to above are most useful.

Analysis of the results show that this technique can be used as a semi-quantitative approach, but relative errors ranging from 10% - 300% are typical. Additionally, due to the mode of analysis required, high probe currents are required to compensate for the 100-fold loss in signal strength. Depth and lateral resolution thus suffer. Finally, the sample must be fully conductive for this analysis to be attempted. Any shift in sample potential due to charging will shift the secondary ion energy distribution accordingly, thus invalidating the approach.

A summary of the major, previously-existing, SIMS quantification methods is provided in Table 1. It can be seen that two methods well-suited for the trace analysis of materials without a well-defined matrix (i.e. semiconductor materials) are the MISR

method and the ion-implanted internal standard approach. The reported range of relative error is smallest for these two quantification schemes when local heterogeneity is not present. Both MISR and the ion-implanted internal standard method have excellent detection limits as compared to the CsM+ and IVM approaches.

B. Imaging Internal Reference Method ("IIR"). As described in the previous section, existing quantification schemes experience varying degrees of success. This can depend to a large extent upon the degree of homogeneity present in a given sample. In order to address the issue of heterogeneity, a method that utilizes the advantages of both the MISR and an internal standard approach has been devised for this work, thus enabling quantification of key phases in heterogeneous samples.

The method relies upon the use of a relative standard, with similar matrix composition for the key phases of interest, mounted within the same SIMS field of view as the unknown. One or more matrix species are imaged, along with the species that define the phases of interest. The regions to be included for a particular analysis are chosen by the analyst as part of the post analysis. Basic image processing and analysis methods are then used to separate the various phases of interest in a given set of images from each other. Ion ratios are then produced in the areas of interest, using either line profiles, or area ratios. Ratios between the standard and the unknown for each field of view are then calculated. Thus, relative concentrations, normalized to at least one matrix species, can be determined between the reference and the unknown

within each field of view. As such, this method will be referred to as the imaging internal reference method ("IIR").

Advantages of the IIR method include:

- This approach avoids instrumental issues of repeatability, much like the ion-implanted internal standard method. Sample tilt, instrumental drift, variable chamber vacuum pressure, and many other variables are experienced in a similar way for both the standard and the unknown.
- The method is simple to implement. Ion implantation is not needed to generate a standard. None of the potential errors involved with ion implantation, such as ion channeling, or implant species backscattering are an issue, as the standard usually is created in a method similar to the unknown. No external calibration curves need to be generated (MISR). No extrapolations of energy distributions need to be calculated (IVM). No loss in instrumental sensitivity is experienced (CsM+). Sensitivity to detector aging is virtually eliminated. Sample charging issues are reduced significantly.
- The technique is applicable to virtually every solid sample type that can be analyzed by SIMS. The use of side-by-side analysis is applicable to metals, polymers, and oxides. Sample types can range from mixtures of particles such as catalysts, to alloys such as steels, to polymers and composites.

- Qualitative imaging SIMS is uniquely able to quickly identify the presence of heterogeneity in a sample. Once a qualitative estimate of the number and types of phases is made, then selection of key elemental species to monitor is generally possible. Additionally, it should be possible at this time to identify likely candidate materials which can be used as relative standards.
- This method is very well-suited to the study of samples where precise determination of relative concentration change is of interest, as well as absolute concentration changes. The accuracy of the results is governed by the judicious choice of reference material, much as is the case in other micro-analytical techniques, such as electron microprobe analysis.

As mentioned previously, the phase of interest in the HSLA model alloys being studied in this work is solid-solution boron. The expected range of composition is between 1 ppm to 12 ppm boron, by weight. The goal in this study was to avoid the analysis of boron-rich precipitates, and to restrict the measurements to micro-regions which contained no detectable precipitates.

The success of any quantitative, image-based approach is dependent upon the data acquisition system and methods employed. Thus a brief discussion of the requirements for quantitative SIMS imaging, and the SIMS image detectors used for this work follows. A more detailed discussion is provided in Appendix A.

IV. Requirements for Quantitative SIMS Image Acquisition

Qualitative direct ion imaging in dynamic SIMS is extremely useful for determining elemental locations and correlations between elements. Transforming the qualitative imaging SIMS into a *quantitative* tool can be accomplished in a variety of ways. The general requirements are as follows:

- Establish an electronically stable detector and acquisition configuration for the acquisition of digital image data (i.e., sensitivity, gain, response, noise, linearity). The foundations for the technology and statistical image processing methods used have been described in basic form previously.[19]
- Define an analysis protocol for the instrumental conditions to achieve the analytical goals (i.e., resolution, sensitivity, magnification, species to be detected).[20]
- Define an algorithm for the digital analysis of the image data (i.e. image processing and analysis methods) that will best achieve the analytical goals (i.e., quantification of specific elemental trends - both in terms of concentration and spatial location).[21]

There are several key parameters to consider in choosing or designing a detector system. These are covered in detail in Appendix B, and include:

A. Ion Image Formation and Conversion. Recall that in the microscope mode of imaging, the secondary ion beam passes through a series of image planes and

focal planes while being filtered in both energy and mass (momentum). The primary ion beam is not focused to a small spot, but rather is defocused onto the sample to provide uniform illumination across the whole field of view. The final image plane is typically projected first onto a *channel plate* (Figures 4 & 5) coupled to a phosphor screen. The resultant visible light image is then typically viewed with a video camera.

A careful consideration of each step of image conversion in a detector system is critical in order to maximize sensitivity, resolution (both lateral and depth), accuracy, and precision of the final image data.

B. Detector resolution. In the microscope mode of operation, final image resolution is typically about 1 μm when imaging a 150 μm field of view. This is quite comparable to the practical resolution of a good light optical microscope.

In cases where sample charging is not a limiting factor, further improvement of the resolution of SIMS images may be possible. Aside from attempting to improve actual ion lens design or ion source design, the most effective means to improve imaging performance is through optimized detector design. In fact, it will be seen that even with the current ion lens design, it is usually the case that SIMS image data effectively loses resolution at the *detection stage*.

Here, the term "detector" is meant to include not only the actual detection sensor, but each component coupled to it. For example, the "channel plate, phosphor screen, and camera" together should be considered a "detector". Image detector lateral resolution is an important consideration in analyzing heterogeneous samples. The ability to discriminate between various phases is directly related to detector

resolution. The subsequent quantification of one phase in the presence of other phases is thus directly related to the ability to identify and isolate those phases in an analysis.

C. **Detector quantum efficiency ("QE")**. The QE of a detector can be defined broadly as the ratio of 'the number of events detected" to "the incident flux of events". Since SIMS is inherently destructive on a local scale, it is important to capture all of the ion data as efficiently as possible. Maintaining a high QE at each stage of image conversion & detection is therefor critical.

This becomes most critical in the detection of trace species which may be present in very small, isolated regions of a given sample. Here the term "small" can be thought of as a region which is at the resolution limit of the technique in all three dimensions (x, y, and z). In the case of dynamic imaging SIMS, this corresponds to an ultimate volume of roughly 0.5 μm x 0.5 μm x 100 Å. Examples include precipitate identification and small phase mapping in steels.

D. **Detector dynamic range**. SIMS is capable of producing data with 9 orders of magnitude dynamic range. Just as for resolution and efficiency, all stages of the detection chain should be examined for factors that could limit dynamic range. The ideal image detector would be able to simultaneously detect very weak data and very intense data in the same image, with high resolution and high speed, at every stage of image conversion.

High dynamic range in a detector system is extremely useful for comparing data between images of trace and matrix species. In these inter-scene situations, it is routine to encounter a range of intensities greater than 10^6:1. As the technique

developed here relies upon image ratios, a large dynamic range will greatly optimize the use of the method.

E. Detector Linearity. The response function of any detector needs to be determined if quantitative results are to be extracted. In the case of video-based imaging detectors, unpredictable non-linearity is a key concern. If non-linear gain can be characterized, predicted, and is reproducible, then a protocol can usually be developed to correct for the linear behavior. Some effort at identifying non-linear effects needs to be made within the range of operating conditions for any quantitative method. Otherwise errors will result.

Non-linear gain can manifest itself both across the field of view, and from image-to-image as a function of illumination (signal strength). The use of a CCD-based camera (either slow scan or video rate) as opposed to a tube-based video camera (i.e. SIT's or ISIT's) does improve the linearity of the final stage of detection. However, the response of the channel plate and phosphor screen need to be characterized as well.

F. Detector frame rate. In the case of cameras for SIMS, the key consideration in choosing a high frame rate camera over a slower, scientific-grade camera is a simple one: real time operation of the microscope. Slow scan CCD cameras provide certain advantages in terms of bit depth and resolution, but practical issues of microscope operation and alignment become significant limitations without a video-rate device. This translates further into a practical ability to maximize the instrumental conditions of sensitivity and lateral resolution for a given analysis.

V. Image Detectors Selected

In choosing a detector, a balance must be struck among several parameters including performance, reliability, serviceability, and final system price. The technical requirements for quantitative SIMS imaging include high frame rate, high resolution, low noise, high bit depth, and extreme sensitivity.

Given the available technology, two customized image detectors were chosen for use in these imaging SIMS studies:

(1) a video rate, intensified, cooled CCD camera; and

(2) a direct ion counting, position sensitive detector known as the resistive anode encoder.

A. Video Intensified Cooled CCD Camera ("VICCD"). The VICCD was custom configured by Princeton Instruments, and provides extreme sensitivity (single ion counting), low noise (signal to noise = 200:1 with single photon sensitivity), moderate resolution (640 x 480 pixels), video-based SIMS imaging. More details regarding this camera design and performance are found in Appendix B.

B. The Resistive Anode Encoder ("RAE"). The high dynamic range (10^9) of SIMS data poses a significant challenge for any imaging detector. Additionally, relating a video-based pixel intensity to actual ion counts can be quite difficult. The loss of resolution inherent in a multi-stage image conversion system, such as is traditionally used in SIMS imaging, can be problematic. Thus, the use of a direct ion

image detector, with ion counts represented directly as pixel values has significant value in SIMS imaging.

The RAE is shown schematically below (Figure 6). The detector sensor assembly (Figure 7) is mounted inside the secondary ion column, directly in the path of the secondary ion beam. The input stage of the standard detector is a stack of three channel plates. A single ion striking this stack of channel plates is converted to a pulse of more than 10^6 electrons. Following the channel plates is a resistive sheet (resistive anode) with electrodes located at each of its four corners. Each electron burst strikes the resistive anode, producing a proportional charge pulse at each corner electrode. Detection circuitry reliably calculates the centroid of the electron burst location at rates approaching 10^5 events per second. Images are stored digitally on a computer and can also be displayed in real time through a simultaneous analog output connected to a high speed oscilloscope.

One key advantage of the RAE is detection of ions directly at the ion image plane. Consider again the case for a 150 μm ion image with 0.2 μm resolution, providing 750 x 750 resolved data points. For video imaging with the original Cameca image detector chain, this ion data can not be adequately sampled without applying sufficient magnification to provide a greatly reduced field of view (12 μm). The high resolution version of the RAE employed herein provides adequately sampled, 0.2 μm resolution, digital ion images with an 80 μm field of view.

The high resolution, digital ion images produced with the RAE have pixel values that are actual ion counts, not gray levels as in camera-based imaging. Bit depth is 16 bits/pixel instantaneously, 32 bits/pixel in total.

The RAE also possesses extremely low noise characteristics: less than 10 noise counts per second per image plane (640,000 positional locations). This translates into a per pixel noise level of 1.56×10^{-5} events/sec/pixel. This rivals even the best scientific-grade cooled CCD camera performance.

VI. Determination of Solid-Solution Boron in Model Steel Alloys

A. Experimental. Four samples of model HSLA steels were provided, all of similar composition and three with the same thermo-mechanical treatment history (Table 2) . The formulated chemistry of the alloys predicted bulk boron concentrations of 12 ppm (two samples), 8 ppm, and 0 ppm, respectively. No other constituent compositions were varied from sample to sample. One 12 ppm-B alloy, having undergone a different thermo-mechanical history from the other alloys, exhibited very few precipitates throughout. The other 12 ppm-B alloy exhibited significant boron precipitation at a location corresponding to the centerline of the processed piece. This precipitation was known to be inherited from the casting process. During the casting process, the slab cools from the outside first, thus certain species will preferentially be pushed ahead of the solidification front via constitutional supercooling. The centerline of the cast slab thus is most susceptible to elemental segregation.

Much like carbon, boron has a limited solubility within the iron lattice. However, due to difficulty in boron detection, the Fe-B phase diagram[22,23] (Figure 8) is not nearly as well-understood as the pure binary Fe-C, much less in the alloy in question. The low solubility of boron in iron makes it extremely susceptible to exclusion from the lattice as cooling occurs in the cast slab. The ability to monitor the

concentration of boron in solid-solution as a function of concentration, cooling rate, and processing conditions is thus critical in the effort to prevent centerline precipitation in these alloys.

Since the precipitation varied on a local scale, to understand the differences in precipitate formation it was critical to measure the solid-solution levels of boron in these alloys on a microscopic scale. This measurement needed to be made in regions with high precipitate density, as well as in precipitate-free regions. Due to the extremely low boron concentrations and microscopic nature of the measurements, verification of the boron levels was not possible using other techniques, including ICP, XRF, and Neutron Activation. SIMS has more than adequate sensitivity for boron (low ppb detection limits), but the quantification of low levels, differing by only 4 ppm absolute (30% relative) for the case of 12 ppm-B vs. 8 ppm-B, would be impossible using most other methods. Moreover, as precipitation was known to be an issue, and was variable from the centerline to the outer portions of the piece, non-imaging SIMS techniques would be problematic due to variable matrix effects. The boron precipitates were identified by SIMS to be boron-oxides, which possess extremely high ion yields versus metallic boron in solid-solution.

An image-based analytical approach utilizing one alloy as an internal relative standard was devised to determine the relative boron solid-solution levels in the two alloys. Here, solid-solution is defined as the boron level in regions with no boron-rich precipitates, within the limits of the spatial resolution of the ion image data (typically 6 μm for a 500 μm field of view). The 8 ppm-B sample would be used as a relative

reference, as it revealed very few precipitates when examined by scanning electron microscopy as well as in qualitative SIMS ion imaging. Image processing would be used to exclude the precipitates from the solid-solution measurements.

To maintain the best possible comparisons between the two alloys, they were mounted side by side in the same SIMS mount. Buehler Epo-Thin† epoxy was used for embedding. Wet polishing was performed using silicon carbide grit, down to 1000 grit finish (7 μm grit size; 3.5 μm nominal finish). Careful alignment (within 50 microns) was established so that the centerline regions of both pieces were aligned within the same SIMS field of view (see light optical image, Figure 9). Low magnification imaging (500 μm field of view) was performed to maximize the sampling area for both samples.

The RAE detector was used in low lateral resolution, image depth profiling mode, which provided higher count rate performance (10^5 cps). The positional resolution of the RAE in this mode is only 100 x 100 positions. Individual RAE sub-images were stored with 256x256 pixel resolution, 16 bits in depth. Thus, the data content in the RAE images is limited to 5.0 μm laterally:

$$(500\text{um}) / (100 \text{ resolution elements}) = 5\ \mu\text{m/ element.}$$

Because the data is stored into 256 x 256 arrays, each 5um data point occupies 2.56 pixels.

Typically 300 images per element were obtained for each analysis. Data file sizes were 300Mb. The stacks of image planes were integrated to a maximum bit

† Buehler, 41 Waukeegan Road, Lake Bluff, IL USA 60044

depth of 32 bits in a single accumulated image. For the case of 300 planes, one analysis can *potentially* provide 300 x 16 bits of depth in each elemental image (a maximum ion intensity of 19×10^{6} counts per pixel).

A matrix species was used to normalize the boron signal levels obtained in each sample. This normalization step is crucial to eliminate unwanted variations due to uneven primary beam illumination, sample tilt, surface roughness, and instrumental drift. As iron is the primary matrix species, the dimer of a minor isotope ($^{54}2Fe^{+}$) was used to keep count rates within the linear range of the RAE, and to avoid hydride overlaps at higher isotopic masses. As was seen in the MISR method, the use of molecular species is also a more effective normalization species for matrix effects than a monatomic species. The actual instrumental conditions employed are provided in Table 3.

B. Results. An example of the resultant accumulated RAE boron ion image data is presented in Figure 10. Simple image analysis methods were utilized to exclude the precipitates, thus yielding solid-solution data only.

Efforts were made to choose regions free of precipitates based upon a visual examination of the images. In analyzing the actual line scan data, additional precipitates were visible as excursions well above the baseline plot and were avoided. Calculation of the point-by-point baseline value for the ratio $^{11}B^{+}/^{54}2Fe^{+}$ in each line profile was then performed. Example plots showing the baseline identification is provided in Figures 11 and 12.

Since the entire sample as mounted was almost one-inch across, several areas were analyzed across the full-length of the sample, with $^{11}B^+/^{54}2Fe^+$ ratios determined at each location. A plot of the averaged results for each field analyzed is provided in Figure 13.

The trend of increased solid-solution boron levels in the centerline of the high-B sample indicates that the boron solubility limit has been exceeded in this alloy. Although not yet definitive, some evidence of boron depletion is seen in large regions adjacent to the centerline. In the centerline, the calculated solid-solution concentration is approximately 17 ppm. Importantly, the method presents alloy formulators with the ability to track relative changes in composition to obtain desired physical properties. Where needed, new alloy formulations can be readily checked using the 8 ppm alloy as a relative internal standard.

The average elemental ratio of all measurements excluding resolvable precipitates is in excellent agreement with the ratio of the formulated value for boron of 1.5 (see Table 4). Converting from ratios to actual concentrations is straightforward. The resultant concentration profile is provided as Figure 14.

Analysis of a second pair of samples was also made using the same IIR approach. This time, a new 12 ppm-B model alloy was fabricated using a different processing method designed to minimize precipitation. Qualitative SIMS imaging verified this fact, and repeat analyses showed this sample to have a consistent B/Fe ion ratio versus position. The second sample was fabricated with zero added boron in the melt. Due to previous experience, it was believed that this should correspond to an

approximate concentration of between 1 - 2 ppm of boron. The goal was to measure the "0" ppm-B sample, using the new 12 ppm alloy as a reference.

The 2 samples were analyzed in the same fashion, as the previous pair. Due to the lower counting statistics for the "0" ppm-B alloy, the entire image was used for the analysis (not just line scans). Both video data and RAE date were obtained, on different areas, to compare the quantitative ability of the two detector systems. Precipitates were excluded using image thresholding. The results are shown in figures 25 & 26 (Figures 15 -24 are discussed in the Appendices). Note that the comparison of the video data with the RAE shows quite good agreement between the two detector systems. The predicted range of 1-2 ppm boron was indeed verified by both the RAE and the video analysis (see Table 4 again).

C. Discussion. The boron solid solution measurements are clearly within the expected range of values for both sets of samples: 1-2 ppm for the "0" ppm alloy, and 11.8 ppm for the "12" ppm alloy. At present, the uncertainty in these numbers is largely due to the lack of similar measurements on other alloys, rather than ion counting errors. As seen in a typical line profile (refer to Figure 12), the resultant additive counting errors [†] are below 4 % in a single pixel. These errors then propagate one step further as an additional ratio must be taken (unknown vs. internal reference). In this case, the maximum error per pixel is on the order of 8%.

Increasing the statistical quality of each pixel measurement is a simple matter in the case of SIMS image data. One may perform line profiles which are taken across

a "1 x n" pixel rectangular element (now referred to as a "pixel equivalent"). Here "n" is chosen (typically in multiples of 10) to increase the total ion counts per pixel equivalent so that adequate counting statistics are obtained. One additional method is to simply acquire the data for longer times. Note that since the pixel equivalent occupies a larger area than a single pixel, care must be taken to avoid the inclusion of unwanted phases in a given line profile analysis.

Further extension of this concept can readily be applied to the entire image, as was done in the case of the "0" ppm alloy. Here, image thresholding was performed on the entire image to exclude unwanted precipitate phases. In the case of boron oxide precipitates, this is very effective since they have significantly higher signal levels that the solid-solution boron phase. The resultant image contains data only from the solid-solution regions, within the resolution limitations of the image. rather than performing a single line profile, one can take advantage of all of the pixels in the image, and the counting statistics of the entire image become commensurately better. Reduction of counting errors to below 1% in the final ratioed image results is routine, even at these trace signal levels.

The inherent image resolution of the ion image data at hand is important to keep in mind before claiming that a successful measurement of solid-solution concentration has been made. This is especially true in the case of precipitates that may be much smaller than 1 μm. However, the utility of the IIR method is not

---

† Recall that counting error estimates for ratios are determined by adding the error in the numerator to the error in the denominator. The error bars indicated in Figure 4 are calculated on a pixel-by-pixel basis. The average error bar in the baseline region is +/- 4%.

restricted to two dimensions. Recalling that the original RAE image data was composed of stacks of 300 individual images, one can explore elemental trends as a function of depth. In this case, the z-direction may give quantitative information with much higher spatial resolution (nominally 100 Å on a local scale), thus complementing the 2-D results already obtained.

Additionally, since we are attempting to relate the solid solution concentration of boron in these alloys to the bulk concentration of boron in these alloys, one must be aware of the relative population densities of the phases of interest. In other words, in these samples, the precipitate density was not significant enough to sequester a large fraction of the total boron added. This is proven to be so by virtue of the fact that we have such excellent correlation with the bulk average boron concentration: even when analyzing "unknowns" with significant numbers of precipitates, relative to reference materials without significant precipitates. However, if bulk concentrations are to be used as the only guideline for determination of a particular phase concentration, then one must be careful to consider the number and frequency of other phases that contain the same species of interest. Combining this information with the expected stoichiometry for each phase will provide an overall estimate as to whether or not the analysis would require corrections for this effect. These corrections should be straightforward using image processing methods to determine the relative area fraction of the various phases, account for stoichiometry, and then estimate the total average concentration of the desired species (say, solid-solution boron) in the sample at hand.

It is also important to note that the technique is a relative method and has only been tested on one system. By using an approach of standard additions, it should be possible to analyze a series of samples of any matrix with increasing concentrations of the species of interest. Once the samples are suitable for other corroborative measurements such as electron microprobe, then the whole suite of quantitative results should be determinable. From the perspective of SIMS quantification, it is clear that the image-based approach holds promise for the analysis of heterogeneous samples. Further work on other systems and additional species is needed to verify the general applicability. The use of the standard addition method outlined above should be a straightforward means to expand the known range of applicability of the IIR method.

VII. Conclusion

The excellent initial results shown for trace, localized boron determination in these steels is encouraging. In terms of the steels at hand, the veracity of the results was adequate to provide real guidance in the subsequently developed processing method so that boron precipitation could be avoided.

The precise nature of this specific study (low standard deviations, and excellent agreement with expected results) is not yet to be taken as a definitive proof that the technique is generally valid. Further studies are planned in other materials systems to test the approach of the IIR method.

The use of image processing methods, sometimes quite simple in nature, is a key component to the extraction of the quantitative results. The quality of the processed results is dependent upon the image acquisition system employed. While outstanding results have already been demonstrated, room exist for the use of a higher resolution video camera (while still maintaining the current strengths of sensitivity and low noise). Similarly, a higher resolution, higher throughput RAE would also provide distinct advantages in the use of the IIR method. Both video and RAE detection systems show adequate performance to attempt these types of measurements.

The ability to perform highly-localized, quantitative measurements of trace species is a unique capability that has resulted from this work. No other technique

offers the unique combination of high spatial resolution, extreme elemental sensitivity, isotopic capability, molecular speciation capability, and quantitative performance for the entire periodic table, all in the form of images. As demonstrated for the field of metallurgy, these capabilities can be combined to quantitatively address important materials science questions which were previously impossible to answer.

Appendix A

Issues in Quantitative SIMS Image Acquisition

Qualitative direct ion imaging in dynamic SIMS is extremely useful for determining elemental locations and correlations between elements. Transforming the qualitative imaging SIMS into a *quantitative* tool can be accomplished in a variety of ways. The general requirements are as follows:

- Establish an electronically stable detector and acquisition configuration for the acquisition of digital image data (i.e., sensitivity, gain, response, noise, linearity). The foundations for the technology and statistical image processing methods used have been described in basic form previously.[19]
- Define an analysis protocol for the instrumental conditions to achieve the analytical goals (i.e., resolution, sensitivity, magnification, species to be detected).[24]
- Define an algorithm for the digital analysis of the image data (i.e. image processing and analysis methods) that will best achieve the analytical goals (i.e., quantification of specific elemental trends - both in terms of concentration and spatial location).[25]

A. **Ion Image Formation and Conversion.** Recall that in the microscope mode of imaging, the secondary ion beam passes through a series of image planes and focal planes while being filtered in both energy and mass (momentum). The primary

ion beam is not focused to a small spot, but rather is defocused onto the sample to provide uniform illumination across the whole field of view. The final image plane is typically projected onto a *channel plate* (Figures 4 & 5) coupled to a phosphor screen. The resultant visible light image is then typically viewed with a video camera.

B. Detector Resolution. From a SIMS instrumentation perspective, it is worth noting that three newer generations of the instrument have evolved with numerous new features (the newest referred to as the Cameca 6f). However no actual improvement in *stigmatic* image resolution has occurred. This is a testament to the difficulty in improving the existing ion optics.

In the case of insulators, the ion image resolution is often limited not just by aberrations in the secondary lenses, but by sample charging. Spherical lens aberrations, the result of ion lens design limitations and imperfect lens construction (i.e., machining) are not easily removed. Sample charging can be minimized by a variety of techniques, each with varying degrees of success. In the microscope mode of operation, final image resolution is typically about 1 μm when imaging a 150 μm field of view. This is quite comparable to the practical resolution of a good light optical microscope.

In cases where charging is not a limiting factor, further improvement of the resolution of SIMS images may be possible. Aside from attempting to improve actual ion lens design or ion source design, the most effective means to improve imaging performance is through optimized detector design. In fact, it will be seen that even

with the current ion lens design, it is usually the case that SIMS image data effectively loses resolution at the *detection stage*.

Here, the term "detector" is meant to include not only the actual detection sensor, but each component coupled to it. For example, the "channel plate, phosphor screen, and camera" together should be considered a "detector". Finally, the associated hardware and computers needed to acquire the detector output are a key concern. The detector also must be matched to an appropriate image acquisition and processing system. Thus, several parameters need to be considered and balanced for optimum performance.

The actual Cameca 3F instrumental image resolution limit has been estimated in the past to be in the range of 0.2 to 0.5 μm for a 150 μm field of view[26]. Since between 300 and 750 data points span the 18 mm diameter of the ion image, each "data point" is between 60 μm to 24 μm in diameter, respectively. The preferred image detector needs to be capable of sampling this data without distorting or aliasing the positional information contained within the ion image plane.

Unfortunately, the problem is cumbersome. In the ideal case a detector should oversample image data by at least a factor of two in order to maintain full lateral resolution (i.e., Shannon's Criterion)[27, 28]. Thus, at each *stage* of image conversion, one needs to sample the previous stage's image data at a frequency that is at least a factor of two higher than the data frequency in the previous stage. Restated in terms of pixels, for one stage of image conversion to adequately sample the data in the preceding stage, the pixel density must be twice as high as the previous stage (in both

x and y). Considering an equivalent resolution of 750 "pixels" in the original ion image plane, before it strikes any detector, the theoretical pixel resolution for an ideal camera would be equal to 6000 pixels in both x and y (see Table 5).

In the original instrumental design, however, the channel plate is the first stage of conversion that limits resolution. Original issue channel plate intensifiers supplied with the Cameca 3f, for example, are single 18 mm channel plates coupled to a P20 phosphor-coated glass plate. The pore size in these channel plates is 16 μm, with 25 μm center-to-center spacing. The theoretical resolution of these channel plates is quoted as 20 line pairs per millimeter ("lp/mm")[†], which translates into 720 pixels across the entire 18mm image. This channel plate thus undersamples the ion image plane by a factor of (750x2) / 720 = 2.1.

For glass substrate phosphor screens, the transmission resolution is limited by the size of the individual phosphor crystals and the thickness of the phosphor layer. Ideally, the phosphor layer is applied using a spin coating technique which yields a monolayer of phosphor crystals onto the glass plate. The original Cameca phosphor crystal size ranged from 1 μm to 10 μm (Figure 15). The original phosphor layer was several crystals thick, as spin coating was not employed.

The actual resolution (in both x and y) at each stage of the original Cameca SIMS image conversion process is estimated in Table 6. Here it is seen that the

---

[†] This unit of resolution "lp/mm" or "line pairs per millimeter" originates from a 1951 "Resolving Power Specification" of the US AirForce. This specification was formally embodied as Mil Spec 150A, dated 1959. One line pair is simply "one black line next to an equal width white space", where a series of equally-spaced, equal-width black lines are drawn on a white background One line pair is thus the equivalent of 2 pixels. For channel plates, the limiting resolution is a function of the channel-to-channel spacing, which also determines the smallest possible pore size.

original channel plate, phosphor screen, and standard video camera design each limit the acquisition of full-resolution SIMS images in the direct imaging mode for a 150 μm field-of-view. One operational means to overcome this limitation is to operate the projection lenses in a non-standard mode, providing higher magnification views of the sample. In this case, one simply magnifies the final image prior to any image conversion (i.e., before ions reach the channel plate) by a factor of 2.1. In this case the field of view is limited to 71 μm, and the ion image data is oversampled by a factor of two *at both the channel plate and phosphor screen.* The camera then becomes the only limitation to acquiring full-resolution data for a 71 μm reduced field of view. The required ideal camera resolution in this case is 2880 x 2880 pixels. Using a standard video camera with 640 x 480 pixel resolution, the corresponding ion image field of view would be approximately 12 μm (y-direction).

Higher resolution, high gain, single-stage multi-channel plate/phosphor screen assemblies are now available through Burle Corporation†. The channel plates have 6.5 μm pore diameters with 8 μm center-to-center spacing, 60% open area, and a resolution approaching 70 lp/mm (3500 resolution elements available) across the larger 25 mm image.

The high resolution phosphor screen is composed of spin-coated P20 grains with a size range of 1 μm- 3 μm. The manufacturer's quoted resolution for this screen is 80 lp/mm, which corresponds to 4000 resolution elements.

---

† Burle Electro Optics (previously Galileo Electro Optics) Galileo Park, P.O. Box 550, Sturbridge, MA 01566 USA.

The higher resolution version of the multi-channel plate/phosphor screen assembly has been retrofitted to the SIMS used in this work. As a result, the only limiting stage of image conversion is now the camera, with 6000 x 6000 pixels needed to completely sample the 150 μm image data from the fluorescent screen (Tables 7(a) and (b) , Figure 16).

C. Detector Quantum Efficiency ("QE"). The QE of a detector can be defined broadly as the ratio of the number of events detected to the incident flux of events. For the case of the P20 phosphor, the QE is the number of photons generated per incident electron. The *QE of the P20 phosphor* provided by Burle Electro Optics is specified as 800 photons/electron (for 3 keV electrons). This value is conservative for the Cameca SIMS due to the significantly higher accelerating voltage applied between the channel plate and phosphor screen (15 keV).

For the case of a *CCD camera*, the QE is the ratio of induced electron current in the CCD sensor, to the number of incoming photons impinging upon the front of the CCD. As an example, consider the QE of a typical CCD sensor[29] as a function of wavelength (Figure 17). Visible light SIMS images are projected from the phosphor screen to the camera sensor. Thus, as can be seen in Figure 17, a knowledge of the fluorescent light wavelength is necessary for the phosphor screen to be properly matched to the CCD sensor. Typical SIMS phosphors are P20 with a peak fluorescent wavelength of 560 nm (i.e., green). The corresponding QE of a typical CCD sensor at this wavelength is only 30%. Thus 70% of the photons subtended by the relay optics (camera lens) can be missed due to poor quantum efficiency with a standard CCD.

Since the sample is being sputtered in any SIMS analysis it is critical to detect the secondary ions as efficiently as possible. For example, if the detector needs two ion strikes on average to register an event (i.e., 50% efficient), then twice as much material will need to be sputtered in a given analysis (to obtain the same detection limit & statistical significance) as compared to a detector that detects every ion strike (i.e., 100% efficient). Thus in the total SIMS image detector chain, each component's quantum efficiency affects the minimum required depth of analysis, detection sensitivity, counting precision and time required for analysis.

Chemically etching the backside of a CCD sensor, and then using this thinned backside of the CCD as the detection surface, provides dramatic increases in the QE of the sensor. Unfortunately, this "backthinning" method is expensive and is not possible for all CCD sensors. If backthinning is possible, then quantum efficiencies of 80% or more can be realized (Figure 17).

The use of an *image intensifier* is a method to compensate for poor detector efficiencies. Composed of a channel plate assembly with a photocathode at the input face, and a phosphor screen at the exit face, many photons (10^3 to 10^4) are generated at this phosphor screen for each incoming ion. A tapered fiber optic array is used to couple the intensifier to the camera's CCD array. This intensifier then becomes an intrinsic part of the camera itself. Used in a high-gain, saturation mode, intensified cameras can act as ion counting devices when ion fluxes are low. However, just as with the other portions of the camera, the intensifier assembly needs to be chosen with respect to resolution and QE.

For cameras, signal losses are also affected by the method employed to couple the camera to the SIMS phosphor screen. Coupling efficiency is defined as the number of photons ultimately transferred to the camera input, divided by the number of photons emitted from the phosphor (through 2π steradians). No consideration of photon detection is made in this calculation, but rather how many photons are relayed from one stage to the next. In the case where *lenses* are used to view the screen, signal losses are an inverse function of the numerical aperture of the lens system; thus, low f-stop lenses are preferred. As an alternative to traditional lens coupling, improved coupling efficiency is again realized through the use of tapered fiber optic bundle which is cement-bonded to both the camera sensor (typically a CCD) and the phosphor screen. If the CCD camera is already intensified, then the coupling would be between the SIMS phosphor screen and the input of the intensifier. Unfortunately, fiber optic bundles will suffer from loss in resolution and may introduce image artifacts in the form of either a honeycomb or a random bundle pattern. These patterns are the result of the method by which smaller groups of individual fibers are stacked together prior to being fused into a larger fiber bundle. Because of the need for optically-cemented bonds between the bundle and the CCD or phosphor screen, fiber optic bundles are troublesome to work with if frequent access is needed to the phosphor screen or the camera for servicing.

In summary, for the total ion detector chain the conversion and transmission efficiency of each stage needs to be considered: "channel plate + phosphor + coupling device + camera". If not carefully chosen, significant loss of signal will occur. For

example, where amplification occurs only at the channel plate stage, an estimate of the net efficiency is given in Table 8.

D. **Detector Dynamic Range**. SIMS is capable of producing data with 9 orders of magnitude dynamic range. Just as for resolution and efficiency, all stages of the detection chain should be examined for factors that could limit dynamic range. The ideal image detector would be able to simultaneously detect very weak data and very intense data in the same image, with high resolution and high speed, at every stage of image conversion. In practice this is limited by several factors, including:

- Channel plate-phosphor screen non-linearity, dead time, and saturation in high ion flux conditions.
- Camera dynamic range, data readout rates and data file size.
- Practical issues of storing, manipulating, and processing images above several megabytes in size. Note that this is likely only a temporary concern, as images with 8 to 16 bits of dynamic range and 250,000 - 1,000,000 total pixels are readily handled by today's high-end processors.

As an example, consider the issues surrounding the camera alone. Standard video data has a great advantage for SIMS in that it can be transmitted with 8 bits of linear dynamic range within a single image, and handled by readily available hardware such as VCR's and printers. Non-linear video data (i.e., gamma processed) can display the end points of a larger dynamic range (approaching 10 bits) at the expense of gray-level resolution. A handful of cooled, scientific-grade CCD-based cameras are now emerging with simultaneous digital (i.e., 12 bit, RS-422) and analog (true RS-

170 video) outputs.[†] In general one finds that dynamic range is gained at the expense of other performance assets, such as frame rate and resolution.

It is important to realize that the quoted dynamic range of a camera does not always equal the dynamic range of the data that is contained within the camera signal. Commonplace in the camera industry is to quote signal to noise of the A/D converter used in the camera itself, but it is quite common to find that no true measure of S/N is made on the camera output signal under realistic or standardized conditions. Thus, for example, one may digitally transmit and store image data files with 12 bits of depth that contain data with only 8 bits of useable dynamic range - the remaining 4 bits containing no meaningful gray level information..

Even if the instrumental noise in the SIMS ion data is negligible (a reasonable estimate in most cases) a CCD camera itself will introduce noise as it captures and transmits ("reads out") the pixel data. In the case of non-CCD based cameras such as SIT's or ISIT's[‡], the image data is very noisy when incoming signal levels are low, and camera gains are high. The resultant dynamic range may easily be as low as only 4 bits (16 grey levels) and exhibit a great deal of non-linearity across the image.[30] Due

---

[†] For further information, contact:

Silicon Mountain Design 5055 Corporate Plaza Drive Suite 100 Colorado Springs, CO 80919	Roper Scientific/Princeton Instruments, Inc. 3660 Quakerbridge Road Trenton, NJ 08619

[‡] Silicon Intensified Target ("SIT") or Intensified Silicon Intensified Target ("ISIT") cameras are tube-based, rather than CCD-based. These tube-based cameras possess very high gain characteristics, but suffer from decreased dynamic range.

to its unique design, the video-based imaging system used for the present work maintains 200 gray levels (7 - 8 bits) of depth and high lateral resolution even under very high gain conditions. Details of the improved imaging system are provided in Chapter V.

E. Detector Linearity. The response function of any detector needs to be determined if quantitative results are to be extracted. In the case of video-based imaging detectors, unpredictable non-linearity is a key concern. The effect can manifest itself both across the field of view, and from image-to-image as a function of illumination (signal strength). The use of a CCD-based camera (either slow scan or video rate) as opposed to a tube-based video camera (i.e. SIT's or ISIT's) does improve the linearity of the final stage of detection. However, the response of the channel plate and phosphor screen need to be characterized as well.

For purposes of image-to-image linearity, a complete SIMS imaging system can be compared effectively against the count rate performance of either the secondary electron multiplier ("EM") or faraday cup ("FC"). As both of these ion current detectors are linear at high count rates (employ EM $< 10^5$ cts/sec, employ FC $> 10^5$ cts/sec), they can readily be used to benchmark a given SIMS image detector system.

As an example, the particular video-based system employed herein was characterized by analyzing a plain carbon steel for the ratio 56Fe+/54Fe+ as a function of increasing 56Fe+ signal strength as measured on the electron multiplier. The ratio will remain constant for those count rate regimes where the complete detector system response is linear. Integrated images for each iron isotope were obtained under

identical conditions, so that the only variable was secondary ion signal. Images were acquired in ion-counting mode, where the gains were established so that every ion event was counted as a "white" pixel (using 8-bit instantaneous images). Any data near the noise level (5mv rms as compared to 1volt for the ion data) is discriminated as black, so that extremely high signal-to-noise images can result using image integration techniques. The individual 8-bit images are stored into 32-bit memory, thus enabling very long integration times (6.49 days maximum per image at video rates). Image processing is used on the resultant images to calculate the total ion image ratio results (Figure18). The importance of such a measurement is to define the proper count rate regime under which one can operate and not experience detector system saturation. In this case, for the conditions established, the video detector system as a whole can perform quite well under roughly 2×10^4 cts/sec.

Sources of intra-scene non-linearity can include channel plate aging, camera baseline noise/non-linearity, uneven primary beam illumination, and sample charging. If the channel plate and camera system are properly chosen and maintained, then intra-scene non-linearity can effectively be eliminated by simply acquiring a matrix species image (or several matrix species images). The matrix species image can then be used to normalize all other images via image division.

F. Detector Frame Rate. Frame rate can be discussed in terms of signal to noise, bit depth, and other details of image detector performance. In the case of cameras for SIMS, the key consideration in choosing a high frame rate camera over a slower, scientific-grade camera is a simple one: real time operation of the microscope.

For the actual operation of the SIMS, it is imperative that one be able to visualize very weak ion images in real time. Here, real time means at least 15 frames per second ("fps"). Otherwise, it simply becomes impossible to focus and align the microscope. Thus, the use of slow scan (~ 4fps) CCD's are generally unacceptable due to frame rate limitations. Additionally, the simple functionality of true RS-170 video has significant benefits in storing, transmitting, and displaying data with ease.

Appendix B

Image Detectors Selected

In choosing a detector, a balance must be struck among several parameters including performance, reliability, serviceability, and final system price. The technical requirements for quantitative SIMS imaging include high frame rate, high resolution, low noise, high bit depth, and extreme sensitivity.

Given the above factors to consider in choosing various components of the complete detector chain such as the channel plate and camera for traditional SIMS direct ion imaging, it is obvious that room exists for development of an improved detection scheme. Reducing the number of image conversion stages to one stage would greatly impact the ultimate resolution requirement for the image capture device. Reduction of the number of image conversion stages to one direct detection stage would also provide ion counts at each pixel, rather than shades of gray. Thus, given the available technology, two customized image detectors were chosen for use in these imaging SIMS studies:

(1) a video rate, intensified, cooled CCD camera; and

(2) a direct ion counting, position sensitive detector known as the resistive anode encoder.

A. Video Intensified Cooled CCD Camera ("VICCD").

(i) Video Camera Features. The VICCD was custom configured by Princeton Instruments, and provides extreme sensitivity (single ion counting), low noise (signal to noise = 200:1 with single photon sensitivity), moderate resolution (640 x 480 pixels), video-based SIMS imaging. Computer control via RS-232 permits automated, convenient, precise reproduction of all camera settings. The ability to reproduce settings enables consistent control of camera gain, offset, and noise levels, further enabling quantitative video-based imaging. A manual controller is also provided for user control (and storage) of all camera settings in lieu of, or simultaneously with, the RS-232 control via computer (Figure 19).

Single-photon sensitivity is provided by the use of a GenIV-intensifier, fiber coupled to the cooled, video-rate frame transfer cooled CCD sensor with a pixel format of 774 x 490 pixels. Essentially a commercial design, but the first with its specific features, this camera is commercially available from Roper Scientific. Due to the limited number of pixels in the y direction, full ion image resolution is only possible with smaller ion image diameters (i.e., magnification of the 150 μm field of view).

Note that in the SIMS, the visible ion image exists on the vacuum side of the fluorescent screen (glass plate with P20 phosphor coating). For maximum resolution, relay lenses are focused onto the plane of the phosphor coating, and thus couple the camera to the SIMS image detector chain. The first element of the camera is actually a high resolution GenIV (military spec) intensifier assembly made up of a

photocathode-channel plate-phosphor-fiberoptic minifier bonded directly to the face of the CCD array. All components were chosen to maximize overall performance as indicated in Table 9.

(ii) Video Image Processor and Computing Environment. The use of advanced cameras coupled to image processing hardware and software routines has proven invaluable over the years with imaging SIMS. The previous in-house system[19] utilized a standalone image processing engine coupled to a MicroVax-based image processor. Together, all the components provided excellent functionality: live averaging, N-frame integration, image overlays, and extensive post-processing capability.

Even with the limitations of an older system, the previous system was extremely powerful and enabled complicated analyses to be performed in a reasonable time frame. Replacing the basic functionality of this older system proved very difficult even with today's high-end imaging systems. Only a handful of devices possessed the key attributes identified as necessary for the new image processor:

- Very high quality video frame grabbing.
- Standard video display (RGB, NTSC, RS-170) on a second monitor.
- Real time image processing functions such as:
  - N-frame integration ($1<N<2000$).
  - N-frame averaging.
  - Video overlay of stored image data and live image data.
  - Image math (subtraction, division, etc.) using stored and live data.

- RGB overlay capability.
- Image deconvolution (kernel operations)
- Image contrast and brightness enhancement

- Commercial hardware with long term support likely.
- Standard computer platform as host controller, operating under a multitasking operating system.

Interestingly, the most common users of these types of systems are the military and the medical communities, where accurate, fast, reliable video image data are critical. The final system components chosen are as follows:

- SUN Sparc20/Model 70 host computer. This computing environment provided many advantages, including compatibility with the Cameca SIMS control computer, multitasking operating system, X-windows environment compatible with other software programs already in use throughout the microscopy laboratory, and processing power.
- Imaging Technology Inc. ("ITI") MV150/40 real time image processor.† This image processor is modular in design, provides real time processing capability, and is software controlled. Software provided by ITI to control the image processing hardware utilizes standard ANSI C-code.

The ITI MV150/40 is a VME-based, 40 MHz pipeline, frame grabber and image processor that utilizes dedicated hardware devices to perform certain image processing functions in real time. Examples of the possible

† Imaging Technology Incorporated. 55 Middlesex Turnpike, Bedford, MA 01730.

modules include: frame grabber, convolver, histogram, DSP, and memory. The system can be easily configured to suite a particular application, and can be upgraded over time due to its modular design. The modules are controlled by a motherboard which can also be changed over time if a different bus structure is desired. Thus if a PCI bus was desired over a VME bus in the future, all of the modules and code development would remain intact, but the motherboard would be changed to make the system compatible with the new bus of choice. The image processor is connected directly to the Sparc20 via an S-bus to VME converter.

Advantages of the pipeline architecture include very fast 40 MHz transfer speeds between the various modules in the ITI system, and a parallel computational structure. That is, several modules can operate simultaneously performing their respective functions as the data becomes available, and can transfer their results either to memory, display, or another module for subsequent processing (Figure 20).

(iii) Improved Video Data Quality. As stated previously, it can be found that image resolution is quoted simply in terms of the data file size (i.e., 512 x 512 pixels). The actual information content per pixel may not always be considered. In the case of video frame grabbing it is important to evaluate the quality of frame grabber being used - especially for where it is desired that the data be quantifiable.

Consider the following digitized video data. A studio quality video reference signal generator [†] was employed to generate a high resolution modulated reference pattern (Figure 21). The pattern is a sinusoidal pattern with increasing spatial frequency from left to right. It is the type of pattern often used for measuring the modulation transfer function ("MTF") of cameras and optical systems. By virtue of the fact that it is generated electronically, this signal permits the direct evaluation of the entire video acquisition chain independent of the camera used. A separate hardcopy version of the test pattern would typically be used for camera evaluation.

In choosing the final frame grabbing hardware for video acquisition, the above waveform was found to be quite useful. For example, a modern 24-bit video frame grabber card (SUN Sparc20 SUNVideo card) was compared against the ITI MV150/40, and also against the original Crystal Image processor used in our SIMS laboratory. The images and waveform traces obtained are shown below (Figures 22, 23, and 24). The loss of information is readily apparent towards the high frequency side of each image. Two effects are reflected: lack of sampling frequency (i.e., aliasing) and loss of pixel intensity information, which is due to the hardware's inability to track the step changes in intensity (white to black) as the frequency of modulation increases. The ITI MV150/40 demonstrates no significant loss of intensity, but does show some aliasing as the sampling frequency limit is reached.

B. <u>The Resistive Anode Encoder ("RAE")</u>. As already discussed, the high dynamic range of SIMS data poses a significant challenge for any imaging detector.

[†] Model TSG-375A, by SIGMA Electronics, East Petersburg, PA.

Additionally, relating a video-based pixel intensity to actual ion counts can be quite difficult. The loss of resolution inherent in a multi-stage image conversion system, such as is traditionally used in SIMS imaging, has also been shown to be problematic. Thus, the use of a direct ion image detector, with ion counts represented directly as pixel values has significant potential in SIMS imaging.

(i) Standard RAE. The standard RAE has been used in the past by other SIMS researchers with limited success[31]. By working directly with the vendor (Quantar Technology Inc., Santa Cruz, CA) a unique, direct imaging ion detector with specific advantages for SIMS quantitative imaging has resulted.

The RAE is shown schematically (Figure 6). The detector sensor assembly (Figure 7) is mounted inside the secondary ion column, directly in the path of the secondary ion beam. The input stage of the standard detector is a stack of three channel plates. A single ion striking this stack of channel plates is converted to a pulse of more than 10^6 electrons. Following the channel plates is a resistive sheet (resistive anode) with electrodes located at each of its four corners. Each electron burst strikes the resistive anode, producing a proportional charge pulse at each corner electrode. Detection circuitry reliably calculates the centroid of the electron burst location at rates approaching 10^5 events per second. Images are stored digitally on a computer and can also be displayed in real time through a simultaneous analog output connected to a high speed oscilloscope.

(ii) Improved Resolution Dual-Mode RAE. Because the RAE determines the centroid of each electron burst, electron burst spreading at the exit of the channel

plate stack ("blooming") does not limit lateral resolution as in the case of traditional ion imaging. Currently, RAE lateral resolution is limited primarily by the precision of the position measurement circuitry, which is, in turn, limited by the resolution of the 8 bit analog to digital converters ("ADC's") used to digitize the voltage values at each corner of the RAE. The resolution of the traditional RAE is limited to 256 x 256 positional samples, which oversample the ion data to provide reliable 100 x 100 pixel resolution, at total count rates of up to 10^5 ions/sec in the full image. Note that count rates above 10^5 ions/sec can be imaged, but loss of linearity and positional confusion occur due to excessive dead time in the positional circuitry.

The unique RAE design employed herein actually uses a stack of five, ultra-high gain channel plates to provide a gain of over 10^7. This increased gain versus the standard RAE provides higher signal strength at the RAE corners. Additionally, the ADC's are now 10-bit, providing improved digitization of the increased signal strengths at the corners of the RAE. Image data files are stored as 1024 x 1024 pixels. The inherent data content of the RAE image is verified at the time of manufacture to be no less than 400 x 400 pixels. The current degree of oversampling (more than a factor of 2) thus provides true 400 x 400 pixel resolution. Maximum quantitative count rate in the high resolution mode is 10^4 counts/sec in the full image (with less than 10% dead time).

A key advantage of the RAE is detection of ions directly at the ion image plane. Consider again the case for a 150 μm ion image with 0.2 μm resolution, providing 750 x 750 resolved data points. For video imaging with the original

Cameca image detector chain, this ion data can not be adequately sampled without applying sufficient magnification to provide a greatly reduced field of view (12 μm). The high resolution version of the RAE employed herein provides adequately sampled, 0.2 μm resolution, digital ion images with an 80 μm field of view.

Additional benefits of the RAE as an image detector include:

- The high resolution, digital ion images produced with the RAE have pixel values that are actual ion counts, not gray levels as in camera-based imaging.
- The RAE possesses extremely low noise characteristics: less than 10 noise counts per second per image plane (640,000 positional locations). This translates into a per pixel noise level of 1.56×10^{-5} events/sec/pixel. This rivals even the best scientific-grade cooled CCD camera performance.
- High quantum efficiency of 80% and large active channel plate area (70%) provide a minimum RAE ion quantum efficiency of 56% ($0.8 \times 0.7 = 0.56$).
- Very low ion count rates provide the best RAE image performance, with single ion detection sensitivity readily achieved.
- In the special case of this RAE, modification of the position analyzer circuitry permits switching between two modes of image acquisition: (1) High resolution mode, with 400 x 400 resolution element imaging. Count rates can reach 10^4 cts/sec and still produce quantitative, linear results (data files stored as 1024 x 1024 pixels); and

(2) Low resolution mode, with 100 x 100 resolution element imaging. Count rates can reach 10^5 cts/sec while still producing quantitative, linear results (data files stored as 256 x 256 pixels).

- This RAE is readily interfaced to the existing control computer for the SIMS. As in the case of the video image acquisition system, the Cameca control computer is a Sparc 20, X-Windows based system. Included with the control software is an interface to accept the RAE digital output and store the image data directly. Through simultaneous control of the mass spectrometer, quantitative RAE images are readily acquired (16 bits deep per plane, 256 x 256 pixel resolution, 100 x 100 image informational resolution). Image depth profiles are also possible by acquiring stacks of 2-D RAE images as the sample is sputtered. Post-processing of the RAE image data permits small area analysis to occur in either 3-D.

Appendix C

Overview of The Infinite Velocity Method

Infinite Velocity Method ("IVM"). [16] For monatomic species, quantum mechanical arguments[32,33] predict an interesting relationship for "secondary ion yield per secondary neutral" ("Y") as a function of both emission angle ("θ", relative to sample normal) and velocity ("v") of the emitted ion:

$$Y^{+/-}(v, \theta) \propto \exp\left[- M \,/\, v \cos(\theta) \right] \qquad \text{Eqn. 1}$$

where "M" is a constant used to describe the effects of the local surface electronic environment on ionization probability, or local chemical matrix effect.

Examination of the exponential term reveals that if the velocity is allowed to reach high values (i.e. infinity) the exponent approaches zero. The ion yield then becomes insensitive to both "M" and "θ". The matrix effect (and angular effect) should thus not have any impact on the ion yield in an analysis taken to the infinite velocity limit.

To utilize this method, measurements of the secondary ion energy distribution for species of interest are converted into "inverse velocity plots". In these plots, the

secondary ion intensity is plotted versus the inverse of the ion velocity (which is determined from the measured kinetic energy).[17] These plots are then used as the first step in applying the IVM, with results that are theoretically free of matrix-induced errors.[18]

For a detailed treatment of the method, the works referred to above are most useful. In summary however, one generates an inverse velocity plot, with corrections made for instrumental transmission, secondary neutral sputter yield, and the isotopic abundance of the element being monitored. One then extrapolates the linear portion of this corrected inverse velocity plot for each element, and determines the intercept value (ion intensity) for the limit of infinite velocity ($1 / v = 0$). A final correction is then applied for detector efficiency as a function of mass. The final, fully corrected intercept values are then directly proportional to the atomic concentration of each element analyzed. The final suite of atomic percentages can then be calculated simply by ratioing to the known atomic concentration of one analyzed matrix species. As such, one can view this technique as "standardless."

Analysis of the results show that this technique can be used as a semi-quantitative approach, but relative errors ranging from 10% - 300% are typical. Additionally, due to the mode of analysis required, high probe currents are required to compensate for the 100-fold loss in signal strength. Depth and lateral resolution thus suffer. Finally, the sample must be fully conductive for this analysis to be attempted. Any shift in sample potential due to charging will shift the secondary ion energy distribution accordingly, thus invalidating the approach.

References

[1] *Metals Handbook, Desk Edition.* American Society for Metals. H. E. Boyer and T. L. Gall, eds. 1985. p 4-60.

[2] H. Willard, et al., *Instrumental methods of Analysis, Seventh Edition.* Wadsworth Publishing Company. 1988.

[3] P.Willich, K.Schiffman. *Electron Probe Microanalysis of Borophosphosilicate Coatings.* Proceedings of the XIIth International Congress for Electron Microscopy (p. 226). 1990. San Francisco Press.

[4] R. Wilson et al . *Secondary Ion Mass Spectrometry, A Practical Handbook for Depth Profiling and Bulk Impurity Analysis.* John Wiley and Sons. 1989.

[5] H. Wolnik, *Optics of Charged Particles.* Academic Press 1987.

[6] *Transmission Electron Energy Loss Spectrometry in Materials Science.* M.M. Disko, C.C. Ahn, and B. Fultz, eds. TMS, Warrendale, PA. 1992.

[7] A. Benninghoven, F.G. Rudenauer, and H.W. Werner, *Secondary Ion Mass Spectrometry - Basic Concepts, Instrumental Aspects, Applications and Trends. Volume 86 in Chemical Analysis: Monographs on Analytical Chemistry and its Applications.* John Wiley and Sons, Inc. 1987.

[8] D.P. Leta and G.H. Morrison. *Ion Implantation for in-situ Quantitative Ion Microprobe Analysis*, Analytical Chemistry, Vol 52, pp. 277-280. 1980.

[9] G.L. Liu et al. *Accurate Secondary Ion Mass Spectrometry Analysis of Shallow Doping Profiles in Si Based On The Internal Standard Method,* J. Vac. Sci. technol. B14(1) (1996).

[10] A.G. Borzenko, et al. *Reference Materials for Quantitative Microprobe Analysis,* Microscopy and Microanalysis, November 1999, pp.29-31.

---

[11] J.D. Ganjei, D.P. Leta, and G.H. Morrison. *Quantitative Ion Probe Measurement Using Matrix Ion Species Ratios.* Analytical Chemistry, Vol 50, No. 2, 1978. (p 285).

[12] F. Michiels, et al, *Acquisition and Quantification of Ion Images with a Camera-Based Detection System and Classical Quantification Algorithms.*, Journal of the American Society for Mass Spectrometry (1990) 1, pp. 37-52.

[13] C.W. Magee, W.L. Harrington, and E.M. Botnick, *On The Use of CsX^+ Cluster Ions for Major Element Depth Profiling in Secondary Ion Mass Spectrometry.* International Journal of Mass Spectrometry and Ion Processes, 103 (1990) pp. 45-56.

[14] P. Willich and R. Bethke, *Quantitative Depth Profiling of Ti-N-C-O Coating Materials Using MCs^+ SIMS.* Secondary Ion Mass Spectrometry - SIMS XI, Gillen et al, eds. (1998) pp. 991-994. John Wiley & Sons. Chichester, England.

[15] T. Mootz, A. Adriaens, and F. Adams,*Investigations on The MCs_2^+ Formation in Secondary Ion Mass Spectrometry.* International Journal of Mass Spectrometry and Ion Processes, 156 (1996) pp. 1-10.

[16] P.A.W. van der Heide, et al. *The Infinite Velocity Method: a New Method for SIMS Quantification.* Surface and Interface Analysis, Vol. 21, pp.747-757 (1994).

[17] P.A.W. van der Heide, *Secondary Ion Inverse Velocity Plots From a Cameca IMS-3F SIMS Instrument.* Surface Science Letters 302 (1994) L312-L318.

[18] R. Losing, N.Reger, F.J. Stadermann, and H.M. Ortner, *Application of the Infinite Velocity Method for the Quantification of Secondary Ion Emissions.* "Secondary Ion Mass Spectrometry, SIMS XI. Proceedings of the Eleventh International Conference on Secondary Ion Mass Spectrometry." Orlando, Florida. Sept 1997. Gillen, Lareau, Bennet, and Stevie, Eds. John Wiley and Sons. (1998).

[19] D.P. Leta, *A High-Resolution, Single Ion Sensitivity Video Sytem for Secondary Ion Microscopy*, in "Springer Series in Chemical Physics 44", A. Beninghoven, R. Colton, D. Simons, and H. Werner, Eds. , Springer-Verlag, Berlin. (1986) p. 232.

[20] D.P. Leta, W. A. Lamberti, et al., *Petroleum Cracking Catalyst Characterization - Secondary Ion Mass Spectrometry Image Processing Methods*, Chapter 17 in "Fluid Catalytic Cracking II - Concepts in Catalyst Design", edited by M. Occelli. American Chemical Society Symposium Series 452. (1991).

[21] D.P. Leta, W. A. Lamberti, et al., *SIMS Image Processing Methods for Phase Identification and Multiple-Particle Analysis of Small Catalyst Particles*, in proceedings of "Secondary Ion Mass Spectrometry - SIMSVIII", A. Benninghoven et al, eds. John Wiley & Sons. (1991).

[22] W.G. Moffatt. *Handbook of Binary Phase Diagrams.*, Published By General Electric Company, 1983.

[23] *ASM Handbook, Volume 3, Alloy Phase Diagrams.* H. Baker, Ed., ASM International. 1992.

[24] D.P. Leta, W. A. Lamberti, et al., *Petroleum Cracking Catalyst Characterization - Secondary Ion Mass Spectrometry Image Processing Methods*, Chapter 17 in "Fluid Catalytic Cracking II - Concepts in Catalyst Design", edited by M. Occelli. American Chemical Society Symposium Series 452. 1991.

[25] D.P. Leta, W. A. Lamberti, et al., *SIMS Image Processing Methods for Phase Identification and Multiple-Particle Analysis of Small Catalyst Particles*, in proceedings of "Secondary Ion Mass Spectrometry - SIMSVIII", A. Benninghoven et al, eds. John Wiley & Sons. 1991.

[26] M.T. Bernius, et al. *Improved Spatial Resolution of The Cameca IMS-3f Ion Microscope*, "Springer Series in Chemical Physics 44: Secondary Ion Mass Spectrometry: SIMS V", A. Beninghoven, R.J Colton, D.S. Simons, and H.W. Werner, editors, 1986, p. 245-248.

[27] J.C. Russ, *Computer-Assisted Microscopy,* First Edition 1990. p. 29. Plenum Press, New York.

[28] C.E. Shannon, *A Mathematical Theory of Communication.* The Bell System Technical Journal, Vol. 27, pp. 379-423,623-656, July, October, 1948.

[29] Roper Scientific, Inc. On-line Encyclopedia of Imaging, located at web site http://www.prinst.com/library_enc_quantum.shtml. Web site valid as of 5/3/00.

[30] D.P. Leta, W.A. Lamberti et al., *Reliable High Resolution Phase Identification via Imaging SIMS: Subtleties Encountered in Direct and Divided Images,* Abstract in Proceedings of Sixth east Coast Workshop on Secondary Ion Mass Spectrometry. May 20-21, 1993. Held at IBM Corporation, East Fishkill, NY.

[31] R.H. Brigham, et al. *Characterization of Two Resistive Anode Position Sensitive Detectors For Use in Ion Microscopy,* Reviews of Scientific Instruments 64 (2), pp 420 - 429, February 1993.

[32] M. L. Yu, *Work-Function Dependence of negative-Ion Production During Sputtering.* Physical Review Letters, Vol. 40, No. 9, 574 (1978).

[33] J.K. Norskov and B.I. Lundquist. *Secondary-Ion Emission Probability in Sputtering.* Physical Review B, Vol.19, 5661 (1979).

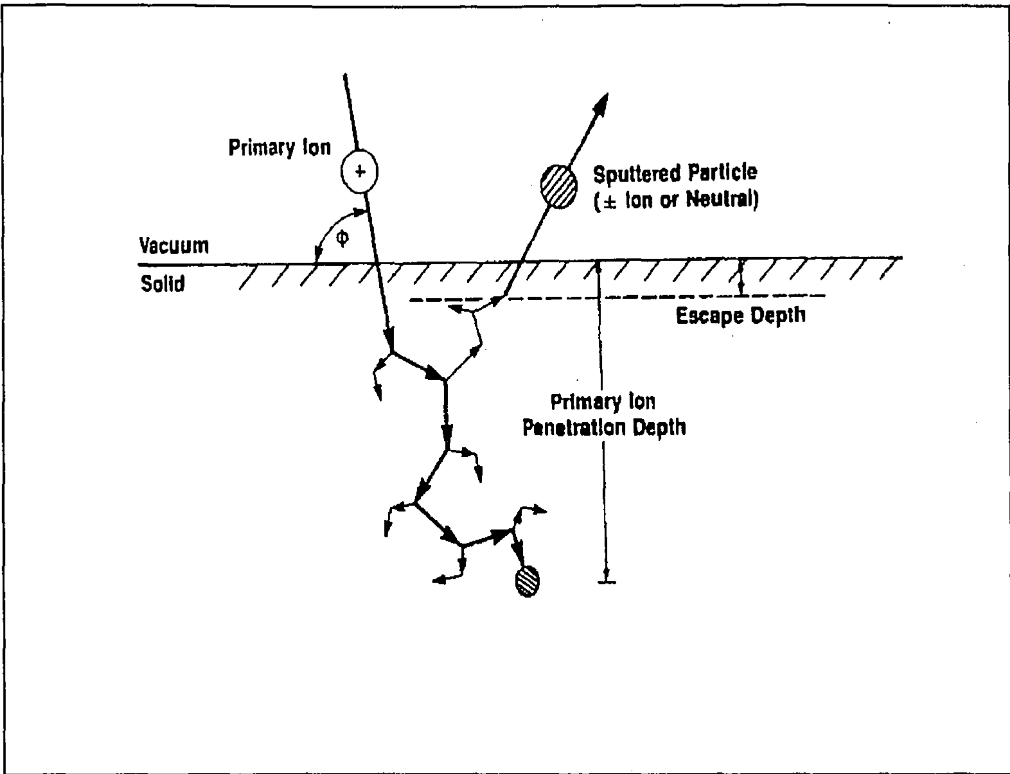

Figure 1. The SIMS sputter process.

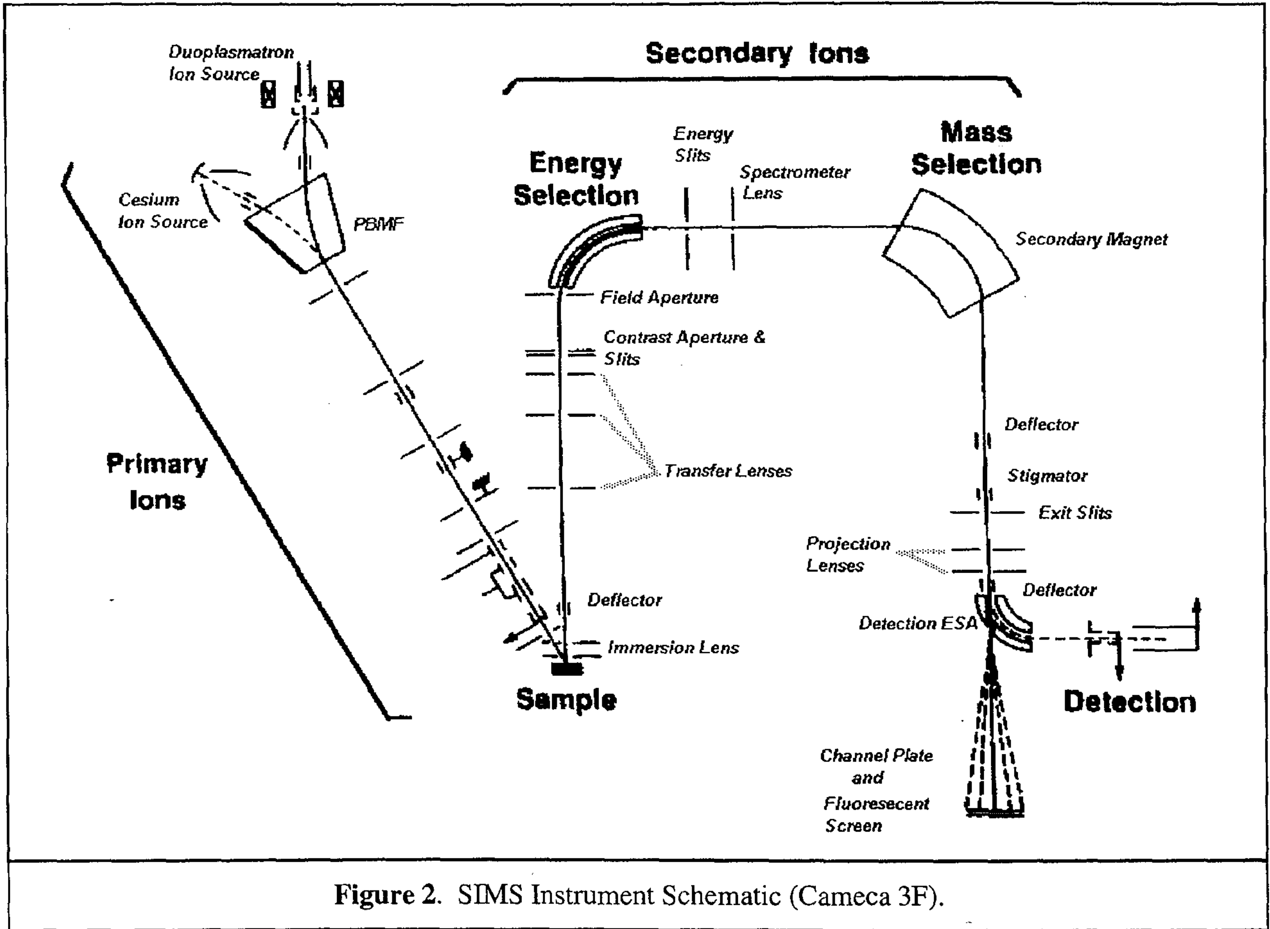

Figure 2. SIMS Instrument Schematic (Cameca 3F).

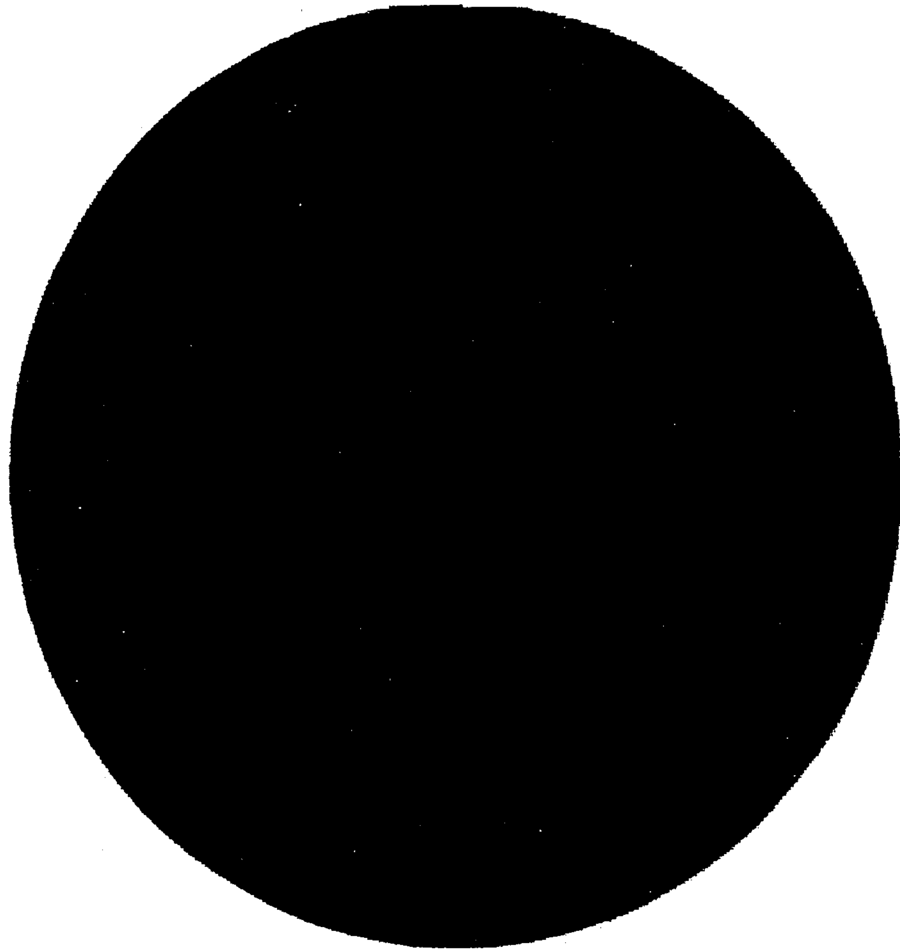

Figure 3. SIMS positive ion images of $^{28}Si^+$, $^{40}Ca^+$, and $^{7}Li^+$ obtained from a commercial reactor lining. Each species is rendered in 8-bits of intensity, within a specific color plane of RGB space. This data was obtained using a Cameca IMS 3f, utilizing an 8keV O_2^+ primary beam, and monitoring positive secondary ions. Image taken in direct ion imaging mode. The diameter of this circular field is approximately 400um.

Figure 3. SIMS positive ion images of $^{28}Si^+$, $^{40}Ca^+$, and $^{7}Li^+$ obtained from a commercial reactor lining. Each species is rendered in 8-bits of intensity, within a specific color plane of RGB space. This data was obtained using a Cameca IMS 3f, utilizing an 8keV O_2^+ primary beam, and monitoring positive secondary ions. Image taken in direct ion imaging mode. The diameter of this circular field is approximately 400um.

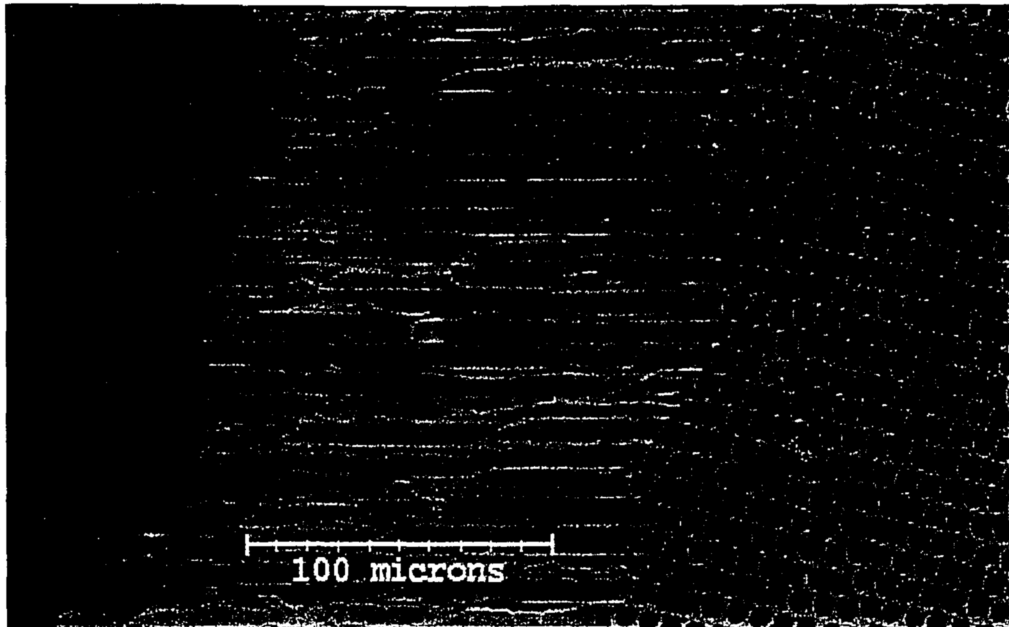

Figure 4: Channel Plate structure as viewed in the SEM. Edge-view of fractured plate reveals internal channels. Input surface pore structure is visible at the right.

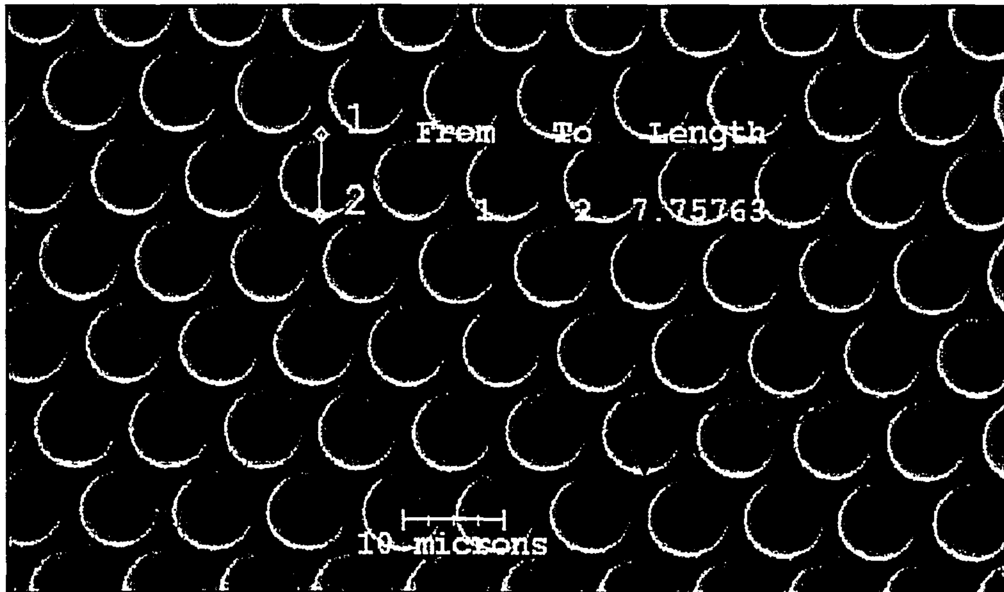

Figure 5. Input surface of channel plate showing nominal pore size (7.8um) and center-to-center spacing (10um). This structure is considered to provide moderately high resolution (50 lp/mm) by today's standards. Note that the "dead" space between pores can become "active" as its dimension is further reduced in higher resolution designs.

INTENTIONAL SECOND EXPOSURE

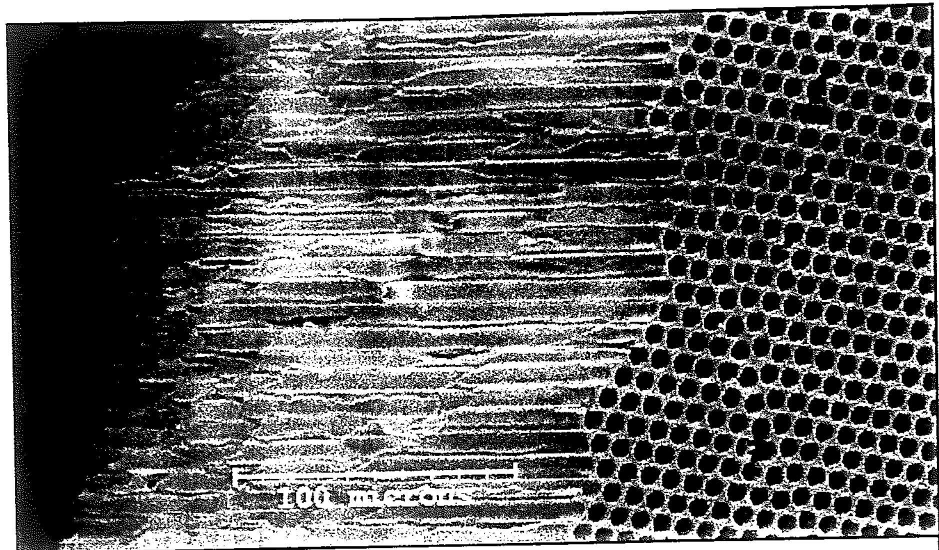

Figure 4: Channel Plate structure as viewed in the SEM. Edge-view of fractured plate reveals internal channels. Input surface pore structure is visible at the right.

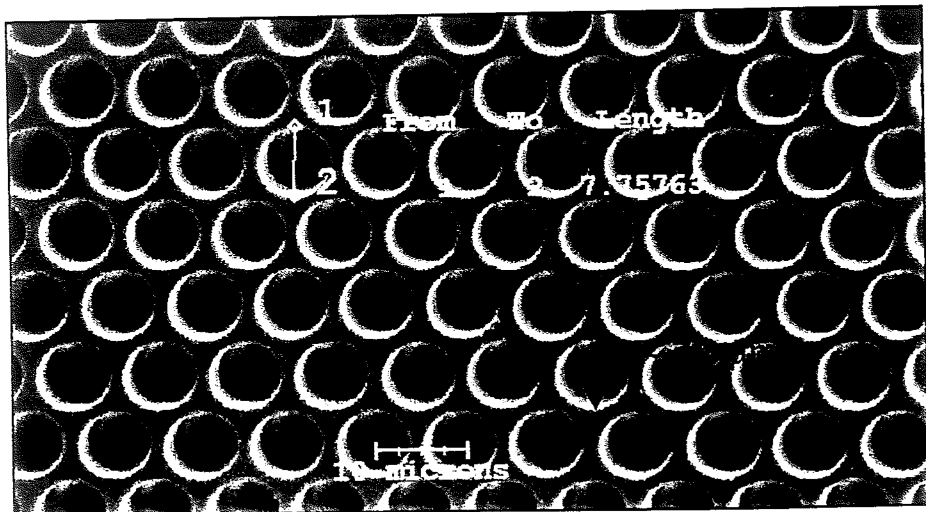

Figure 5. Input surface of channel plate showing nominal pore size (7.8um) and center-to-center spacing (10um). This structure is considered to provide moderately high resolution (50 lp/mm) by today's standards. Note that the "dead" space between pores can become "active" as its dimension is further reduced in higher resolution designs.

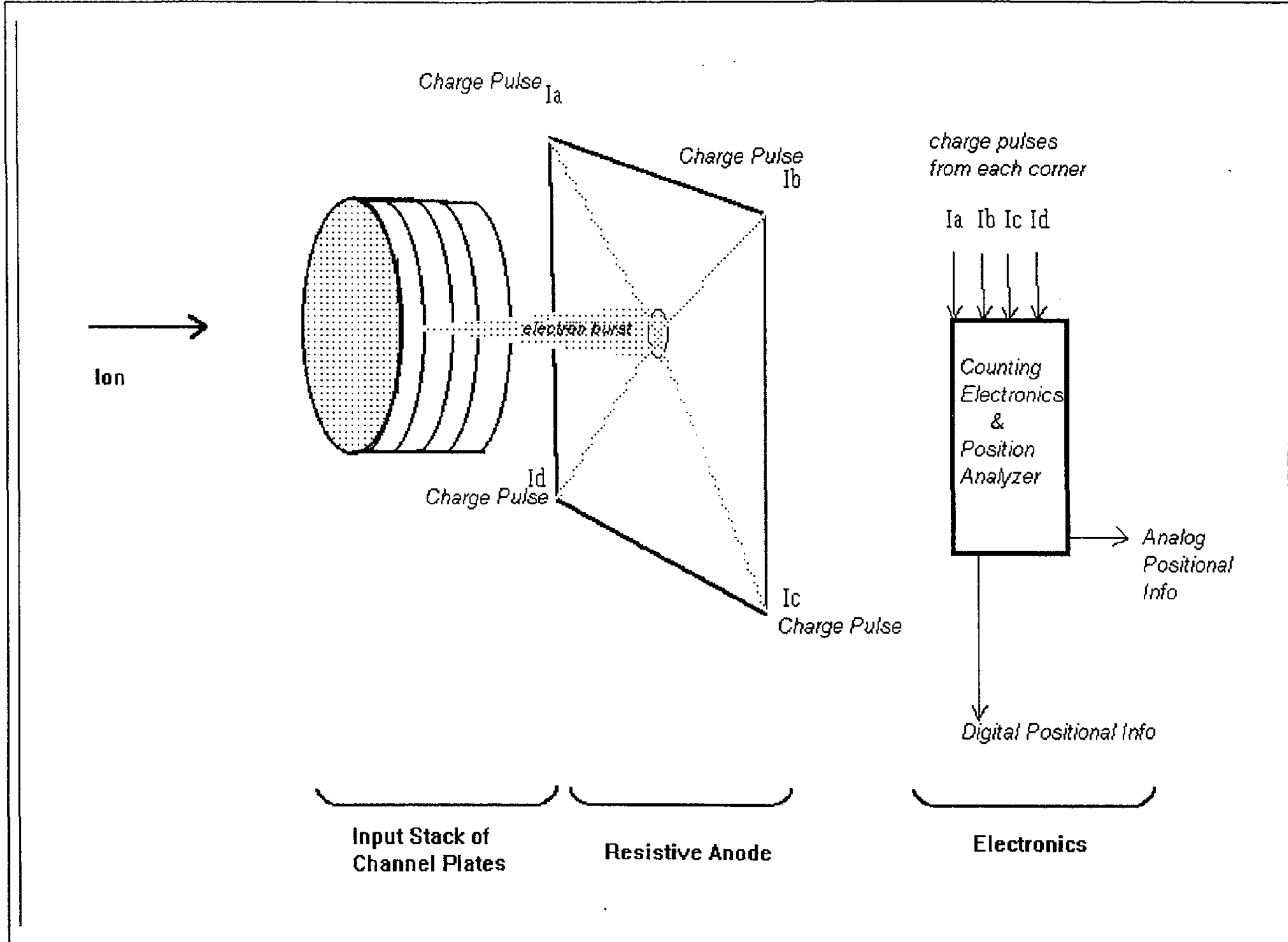

Figure 6. Schematic of Resistive Anode Encoder.

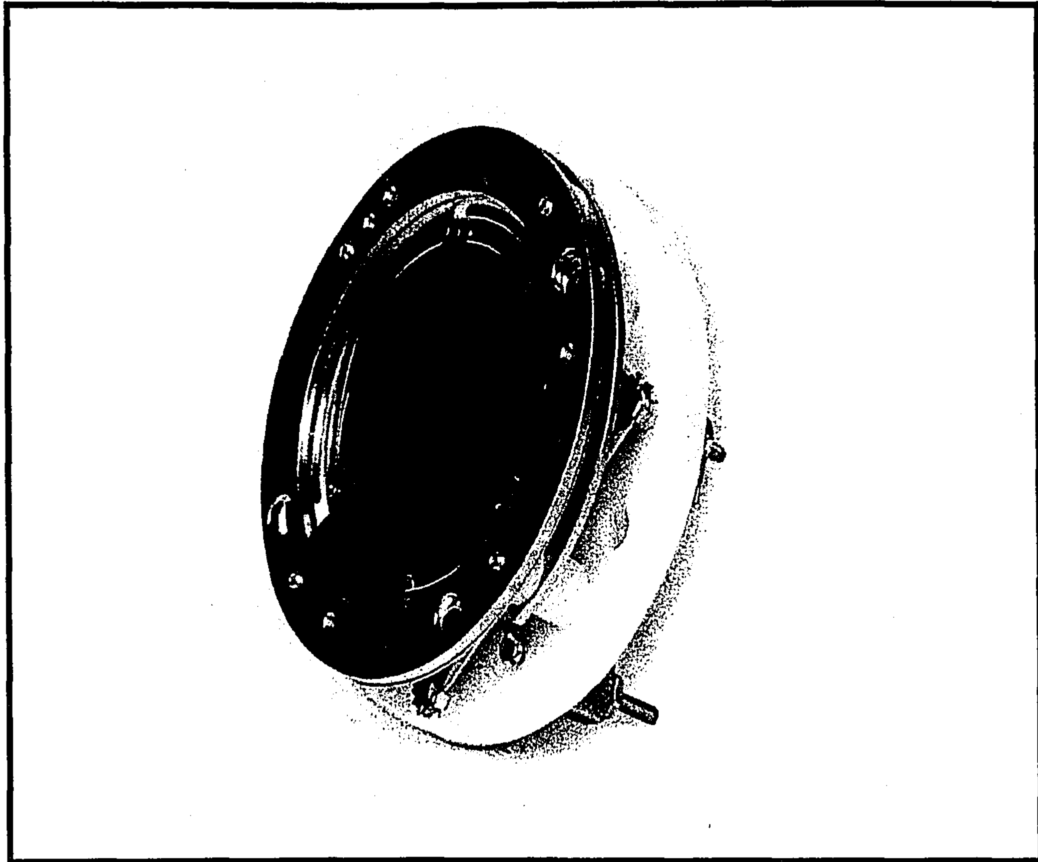

Figure 7. RAE detector sensor. Input face of detector is to the left.

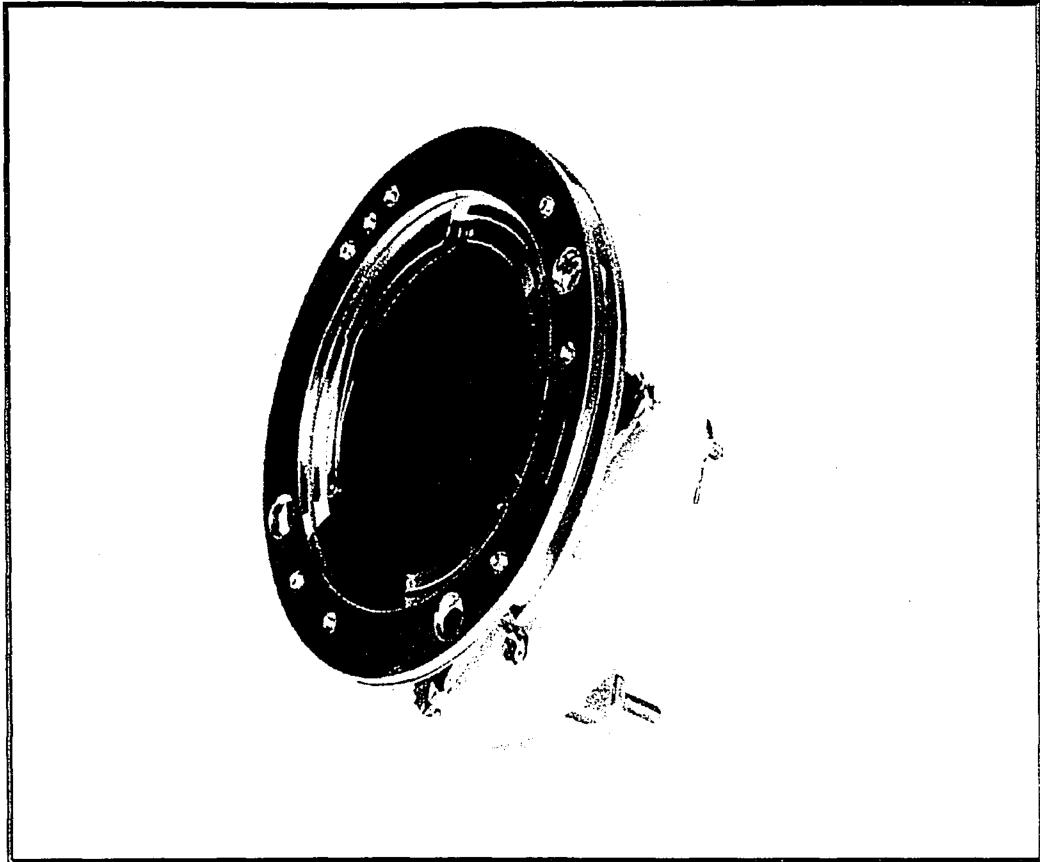

Figure 7. RAE detector sensor. Input face of detector is to the left.

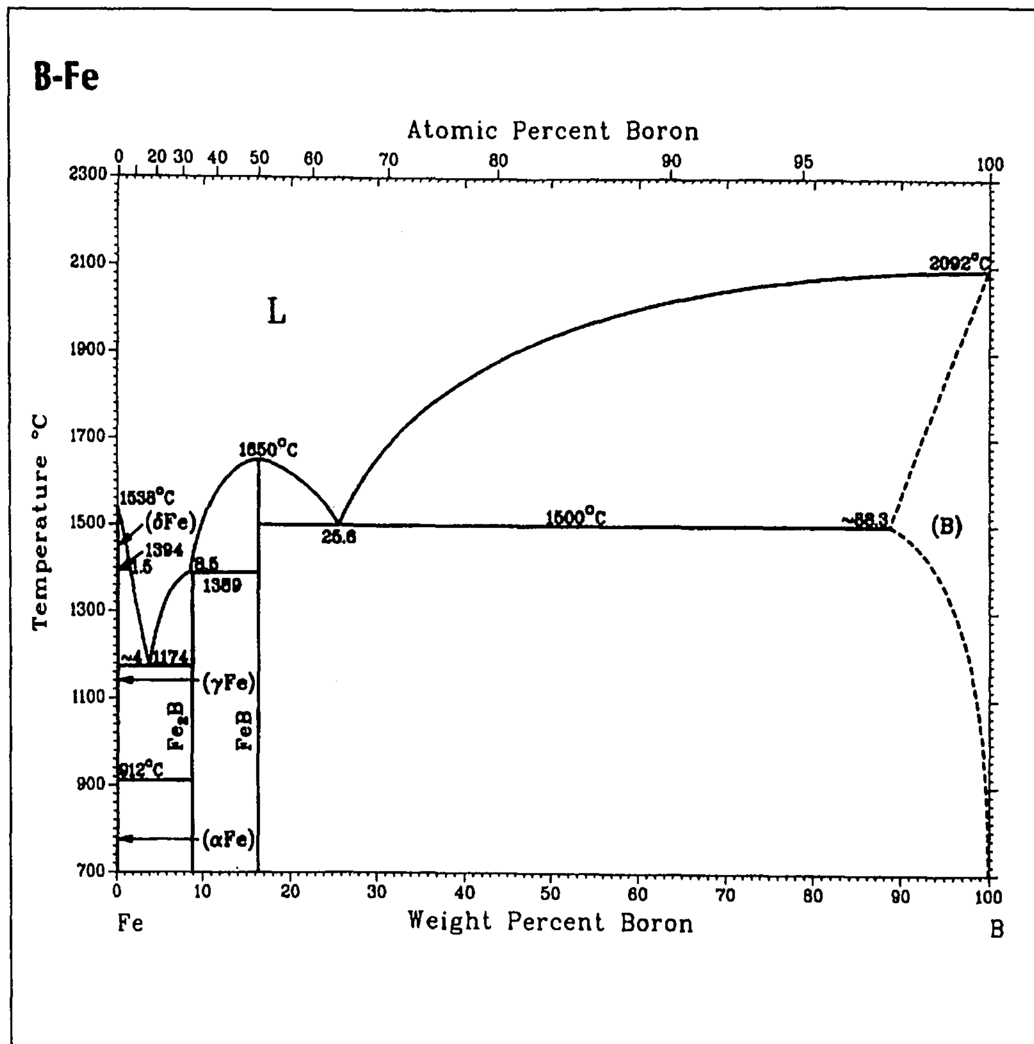

Figure 8. B-Fe phase diagram.

(Obtained from references 27 & 28)

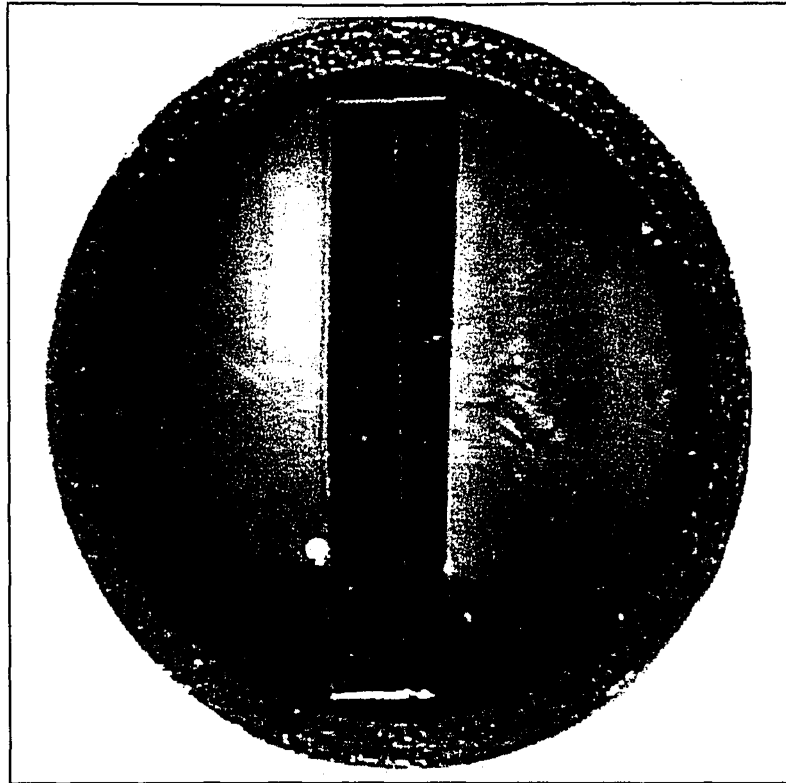

Figure 9. Two alloys, side by side in 1" SIMS mount.

Line Scans Avoiding Precipitates Provide Solid Sol'n Data

Relative Boron Concentration $\propto [\,^{11}B^{+} / \,^{54}2Fe^{+}\,]_{12\,ppm} \;/\; [\,^{11}B^{+} / \,^{54}2Fe^{+}\,]_{8\,ppm}$

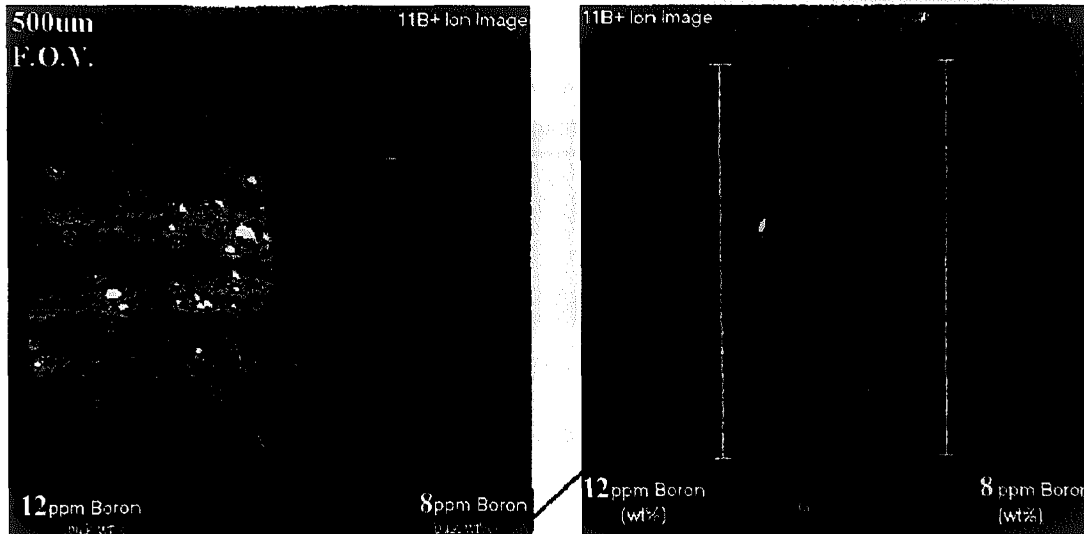

- Line scans are produced.
- Data exported as ASCII files to permit processing
- Exclusions are strictly accurate only for ***"resolvable"*** precipitates.

W.A.L.
p.11

Figure 10. Boron images for both alloys, side by side. Centerline region is in left image pane. Region far from centerline is in right image pane.

INTENTIONAL SECOND EXPOSURE

Line Scans Avoiding Precipitates Provide Solid Sol'n Data

Relative Boron Concentration $\propto [\,^{11}B^+ / \,^{54}2Fe^+\,]_{12\,ppm} \;/\; [\,^{11}B^+ / \,^{54}2Fe^+\,]_{8\,ppm}$

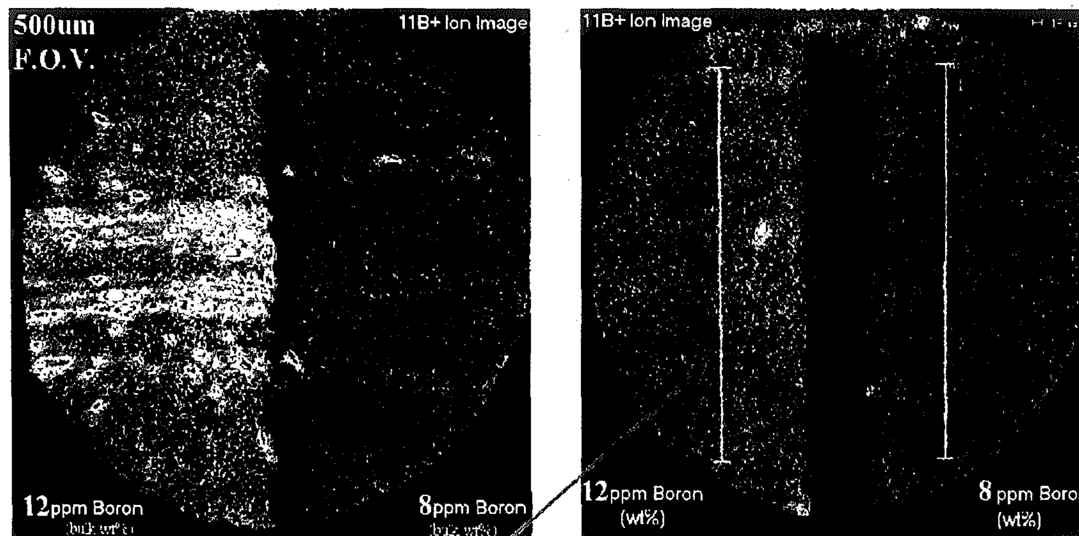

- Line scans are produced.
- Data exported as ASCII files to permit processing
- Exclusions are strictly accurate only for ***"resolvable"*** precipitates.

W.A.L.
p.11

Figure 10. Boron images for both alloys, side by side. Centerline region is in left image pane. Region far from centerline is in right image pane.

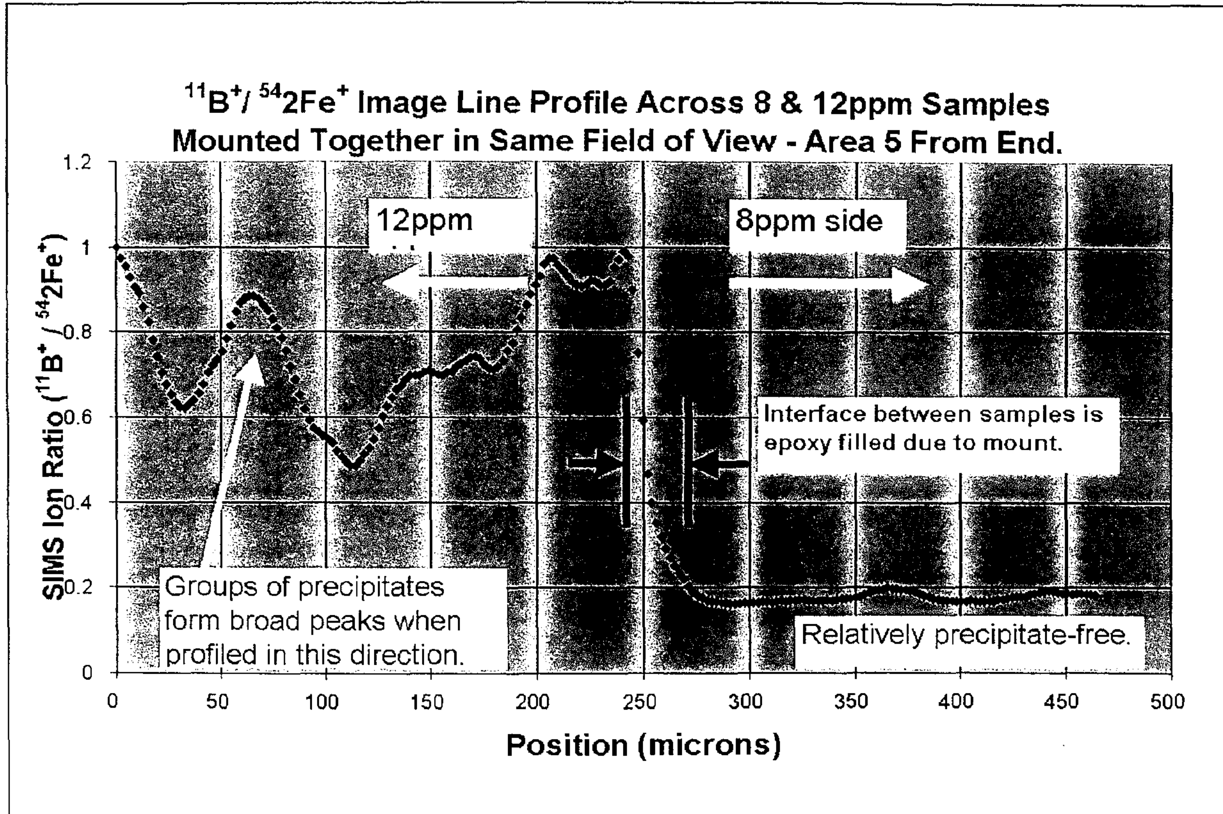

Figure 11. Typical line profile across both samples in SIMS field of view. 12ppm sample is on left. 8ppm sample is on right. Extensive grouping of precipitates on left side is clearly revealed as broad peaks.

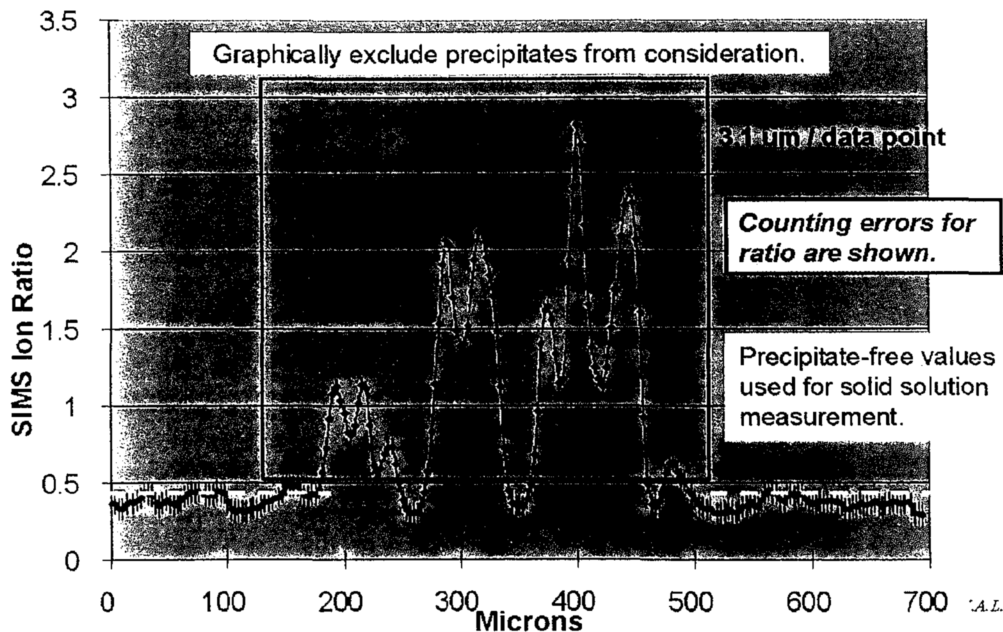

Figure 12. Second line profile across the 12ppm sample alone. Same data field as in figure 18(a) above. Direction is roughly perpendicular to the first line profile. Precipitate grouping is confirmed, and is readily separated from the baseline.

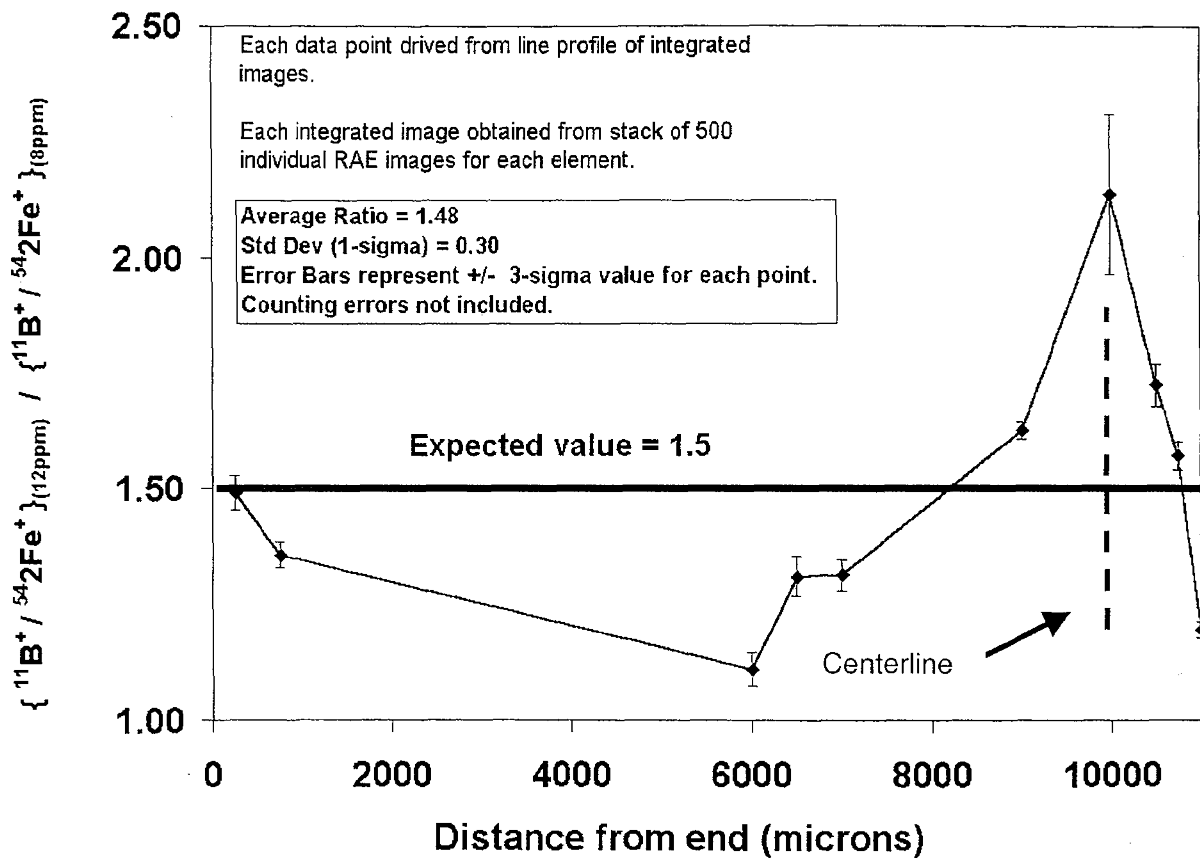

Figure 13. Plot of 12ppm/8ppm $^{11}B^{+}/^{54}2Fe^{+}$ SIMS ion ratios versus position. Increased solid solution levels of boron track precipitate formation. Note that the original alloys were sectioned in half so as to fit within the 1" mount. Thus the original centerline is actually at the far right side of this plot (red dashed line).

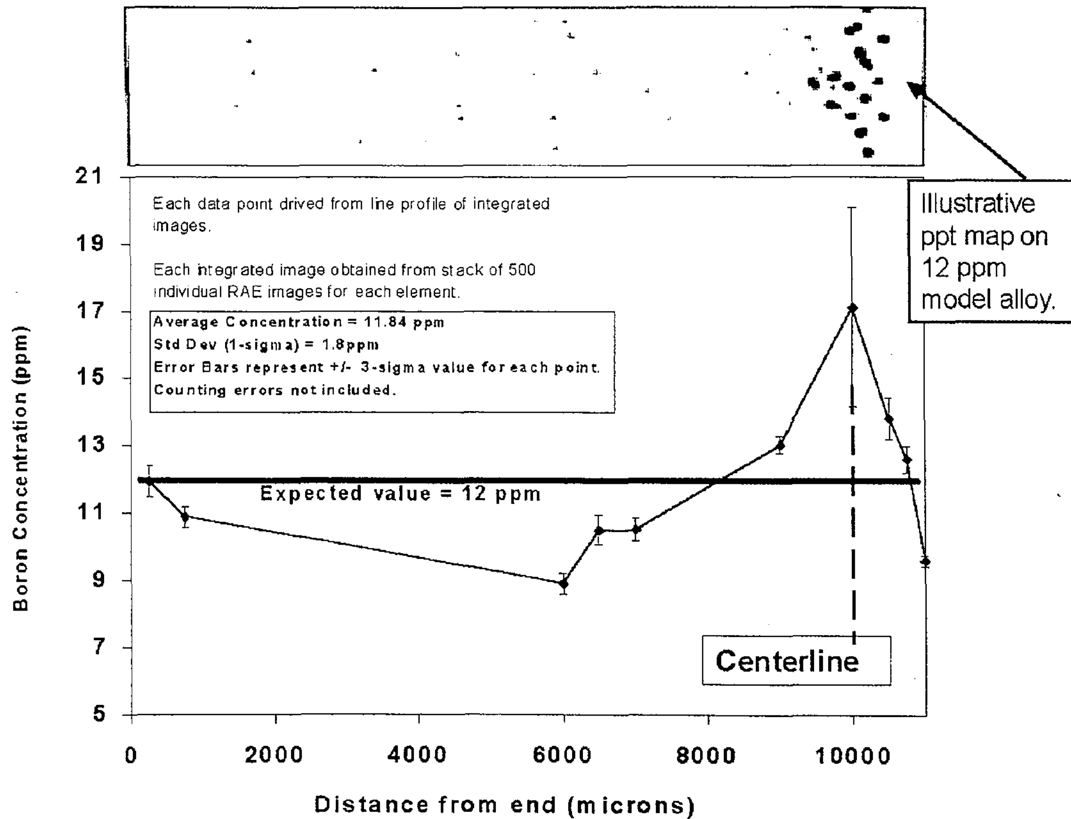

Figure 14. Boron concentration profile obtained by SIMS.

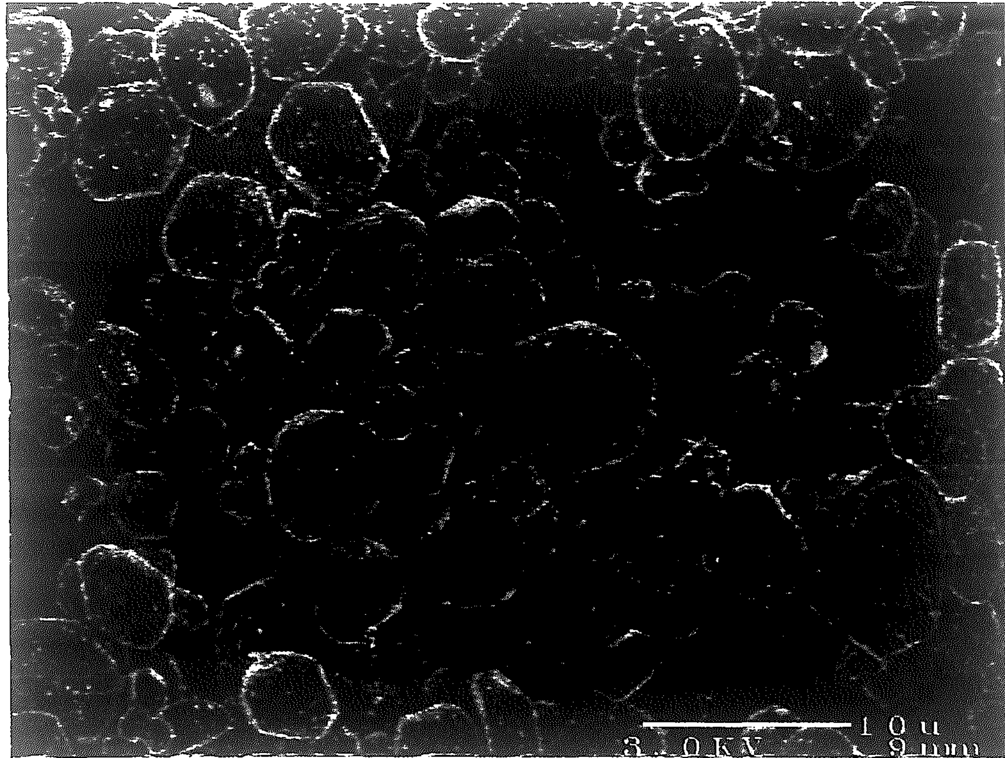

Figure 15. Secondary electron image of original Cameca P20 phosphor grains used on fluorescent screen. Qualitatively it can be seen that the grain size exhibits a braod distribution from 1um - 8 um. This phosphor was rated at 40 lp/mm. The improved design used for this study employ 1um - 3um grains, with a rated resolution of 80 lp/mm.

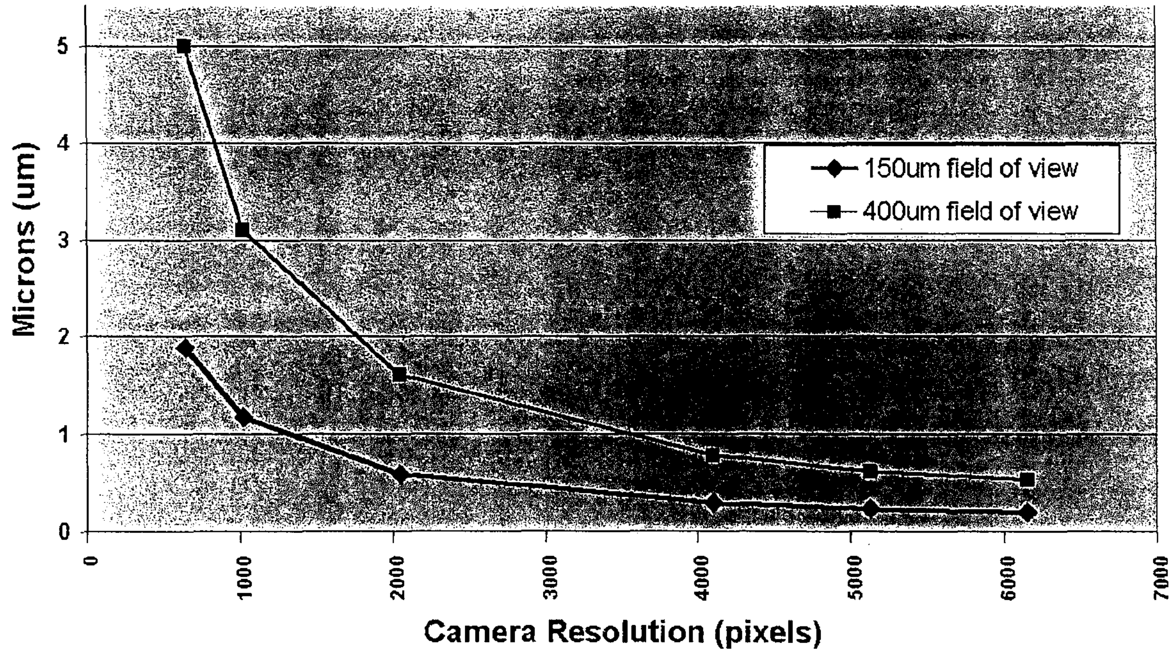

Figure 16. Impact of camera resolution on detected image data content. Also see Table 7(b).

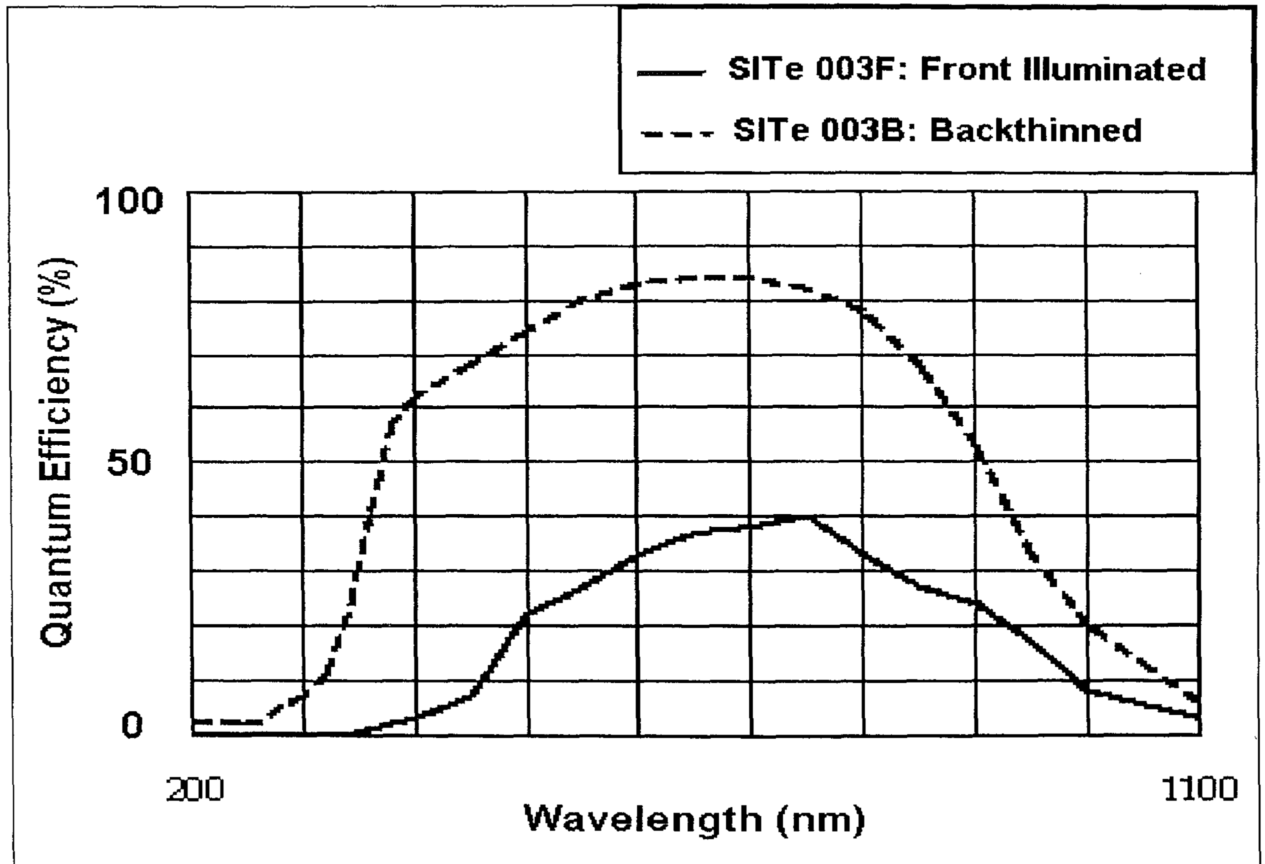

Figure 17. Efficiency curves for typical CCD's. Red (solid) curve is for a front-illuminated CCD. Blue (dashed) is for a backthinned CCD.

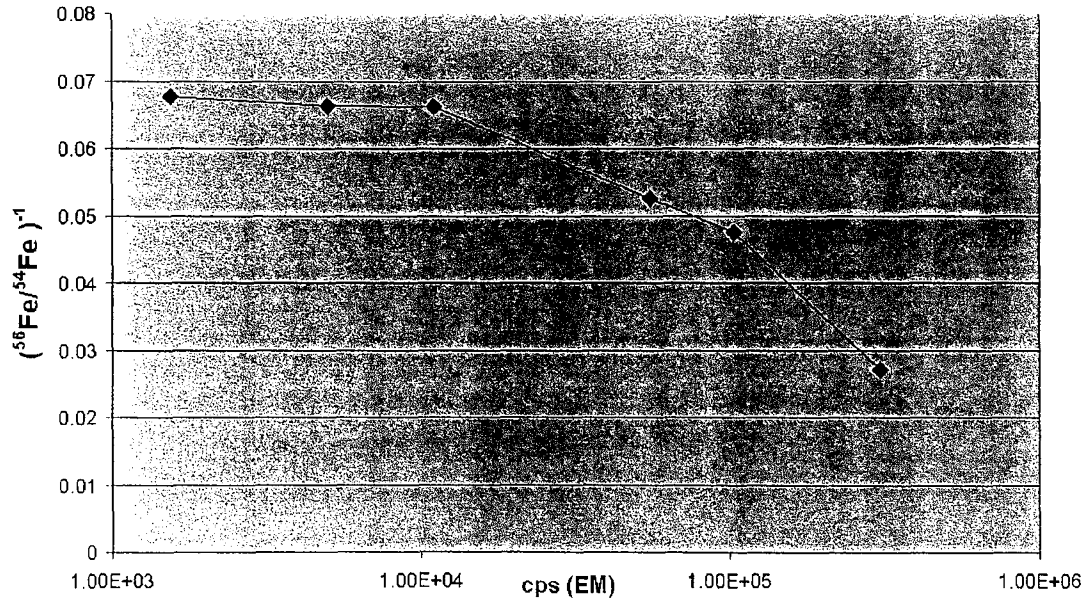

Figure 18. Non-linear response of entire video system is evident above ~ $2x10^4$ cps.

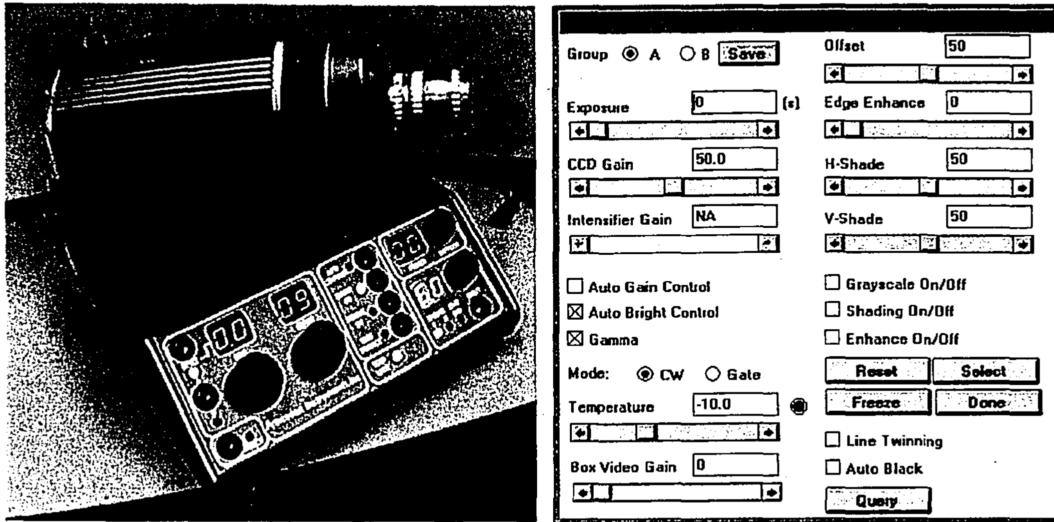

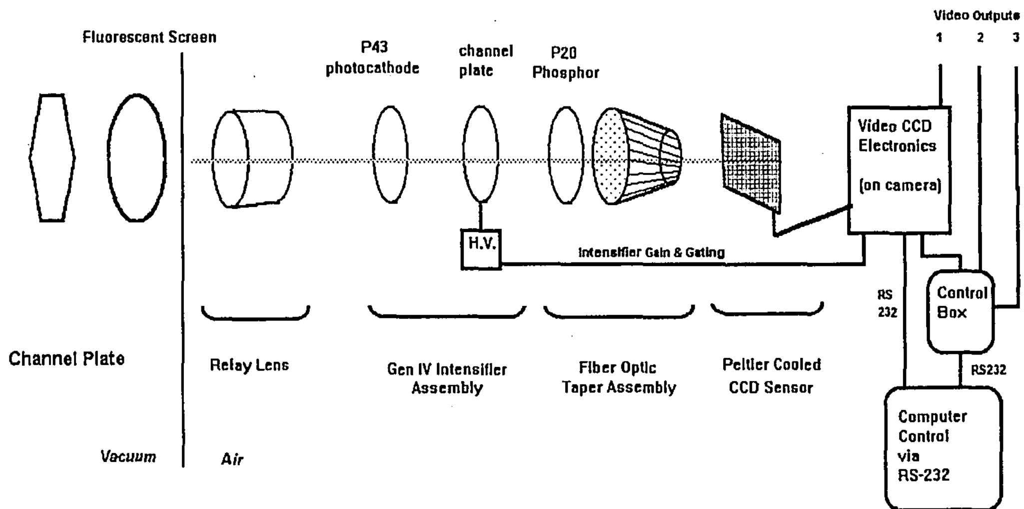

Figure 19. VICCD camera, manual controller, software control panel, and schematic. Response times of each component needs to be kept in same range (Phosphor, channel plate, photocathode, etc.) Slowest time constant will limit deadtime of entire system.

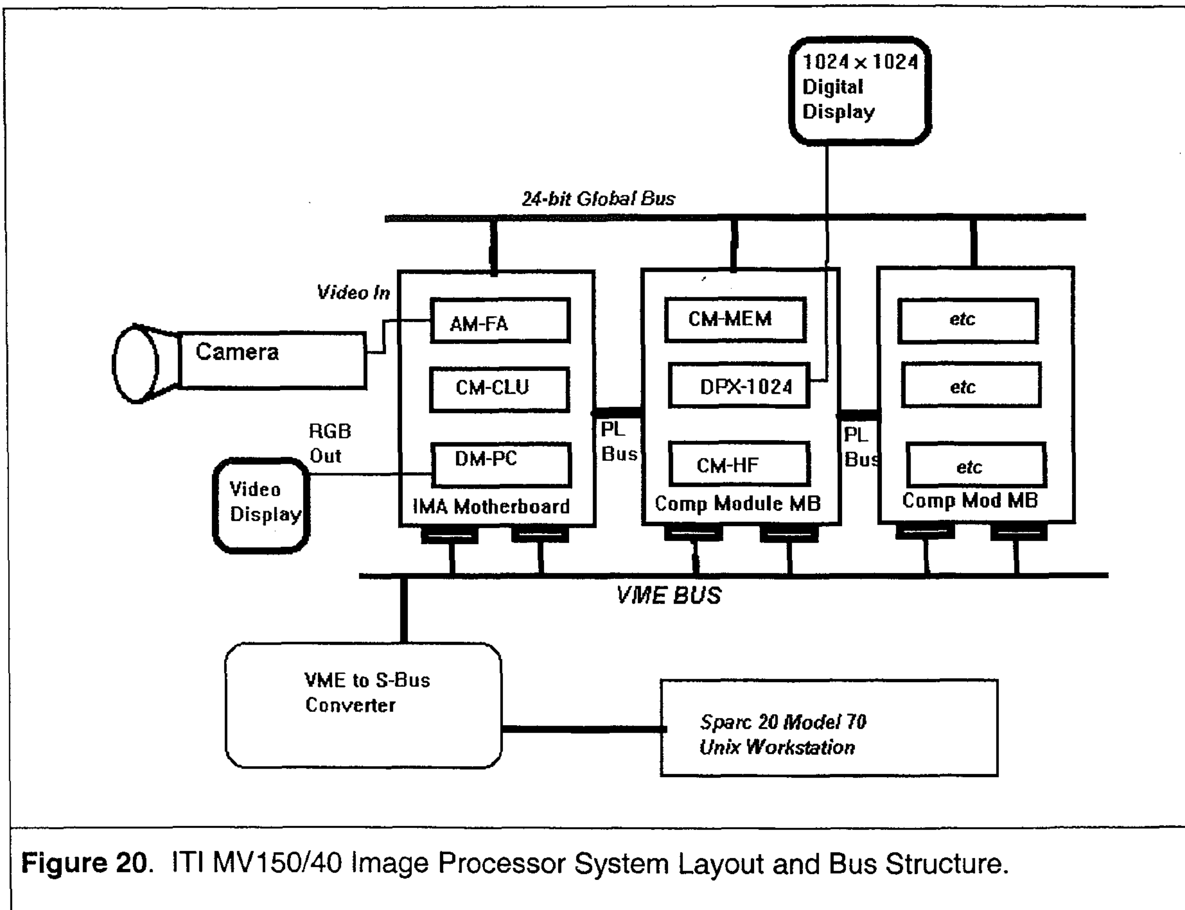

Figure 20. ITI MV150/40 Image Processor System Layout and Bus Structure.

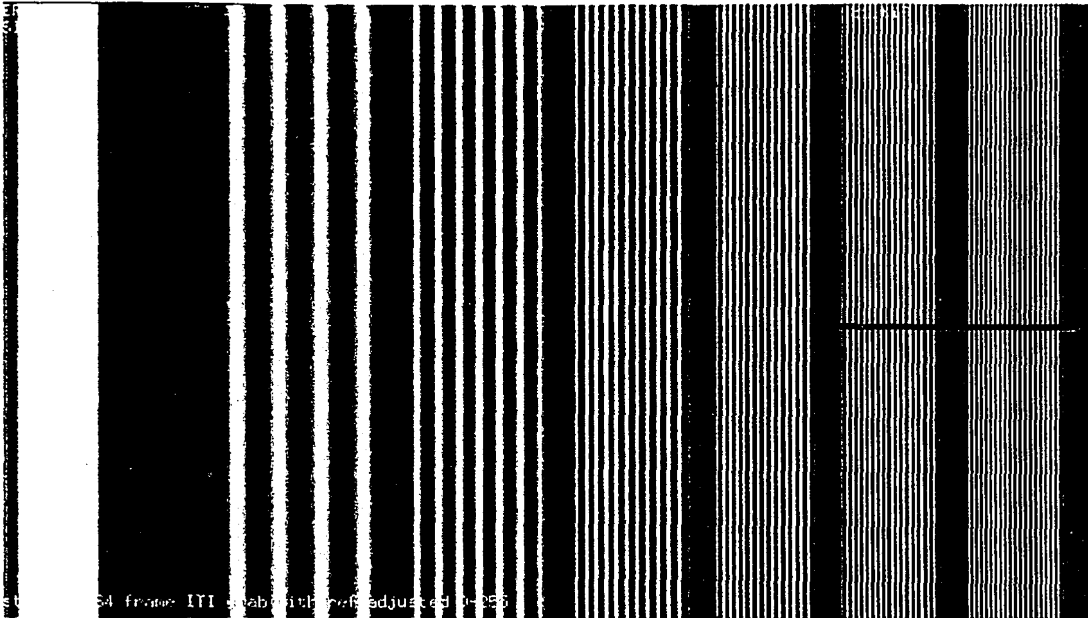

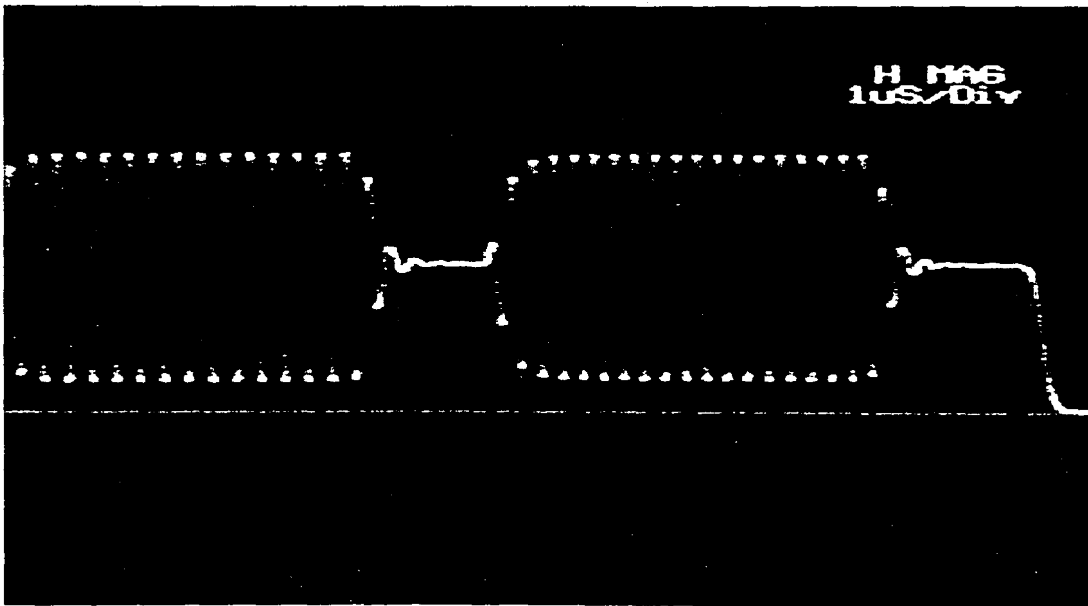

Figure 21. Top frame is reference waveform . Bottom frame is waveform monitor trace of line indicated in red.

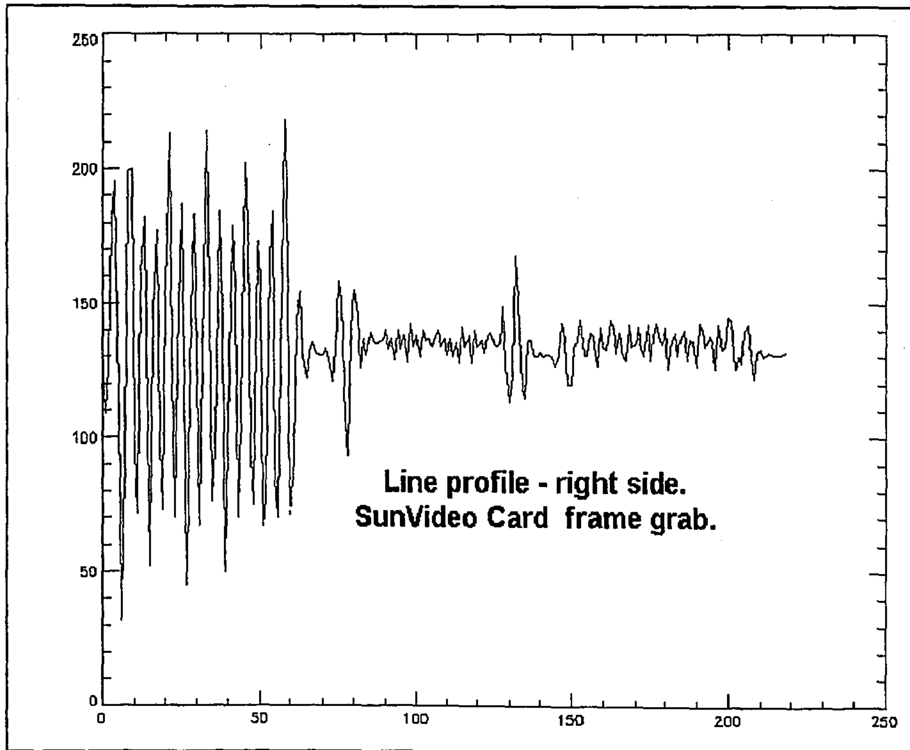

Figure 22. Reference waveform as digitized by the SunVideo frame grabber. Line profile of red path shows loss of data integrity.

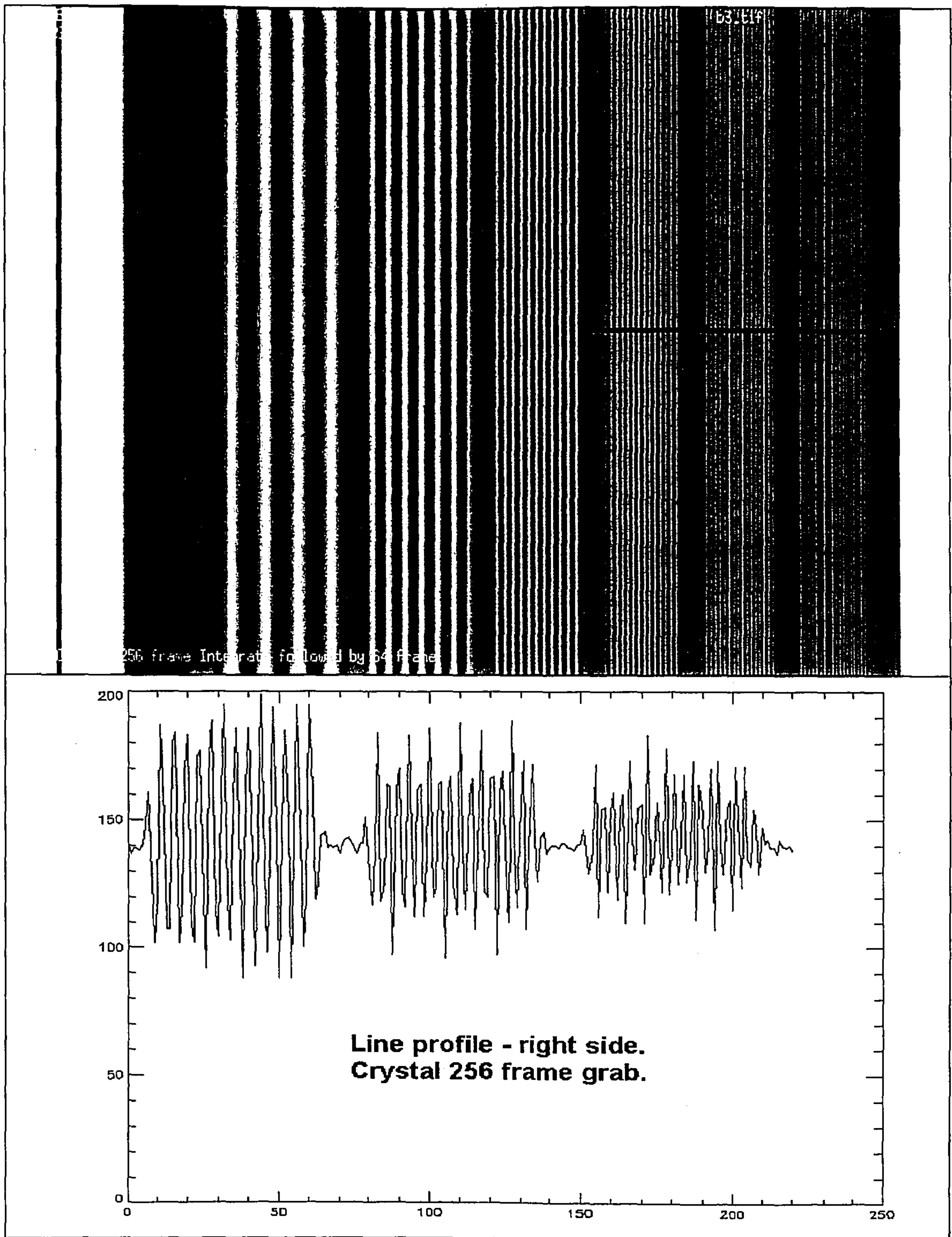

Figure 23. Original Crystal Image Processor (12 years old) shows better fidelity than newer SunVideo card in capturing the highest frequency portions of the waveform. Line profile path indicated in red.

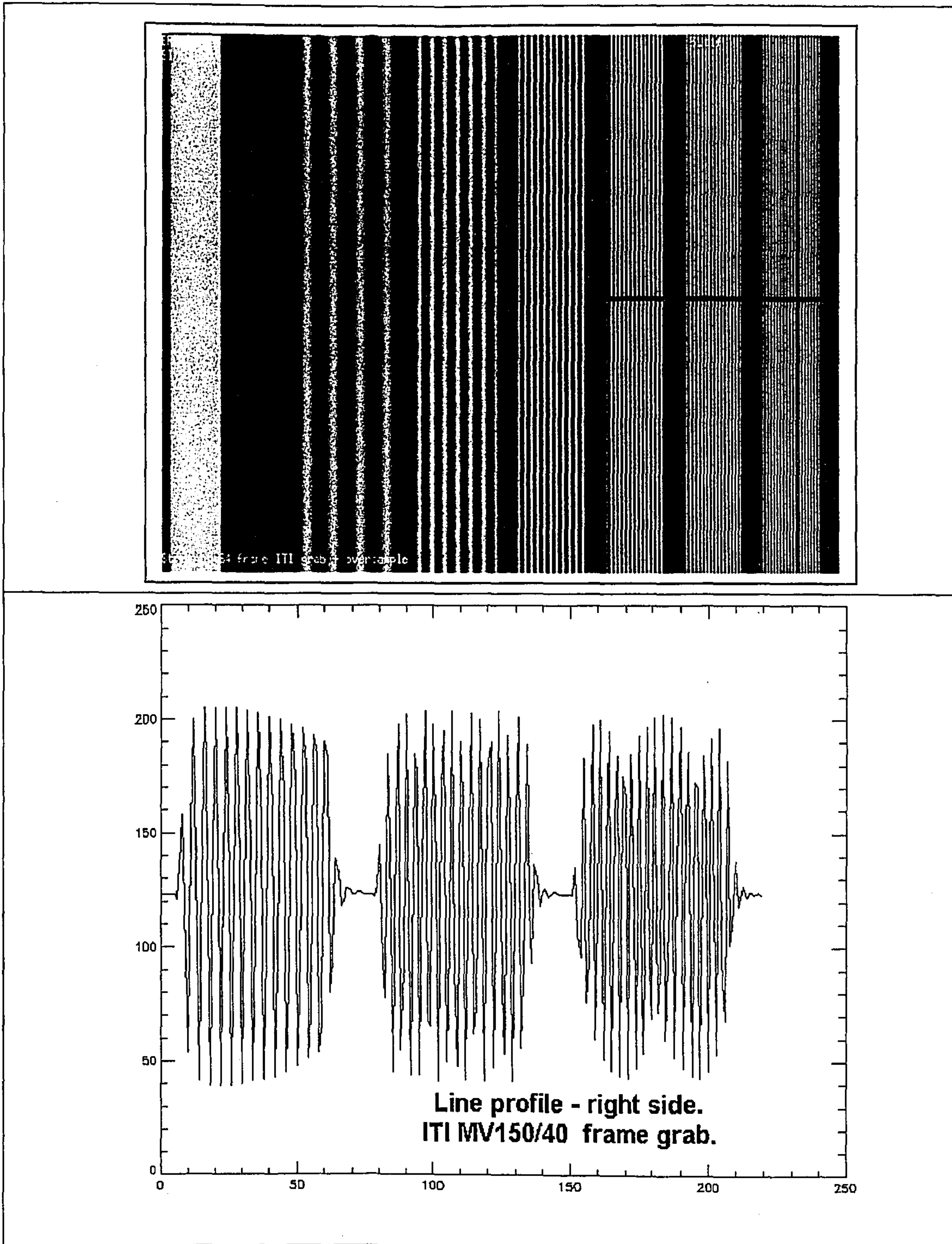

Figure 24. ITI MV150/40 Image Processor maintains the best fidelity in capturing the highest frequency portions of the waveform. Line profile path indicated in red.

Processing of RAE Imaging Data Permits Calculation of Solid Soln B

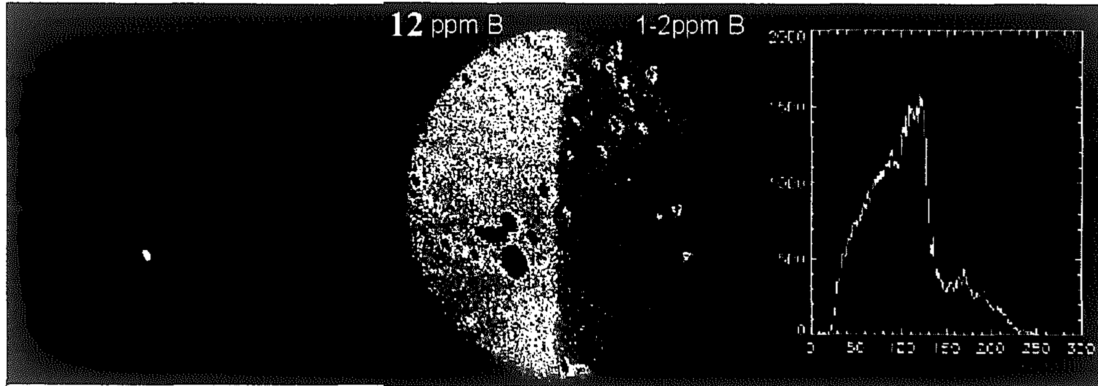

- Utilize 32 bit accumulated data
- Exclude precipitates via image processing
- Calculate integrated Boron line profile for all image rows.
- Sum equal sized individual regions of line-profile for each alloy
- Ratio yields final Boron level = 1.8 ppm

Figure 25. RAE analysis of 12 ppm and "0"ppm samples .

INTENTIONAL SECOND EXPOSURE

Processing of RAE Imaging Data Permits Calculation of Solid Soln B

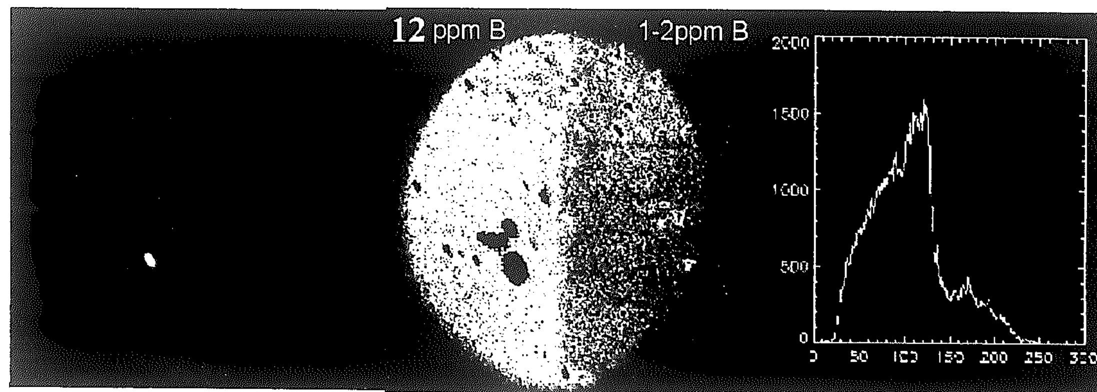

- Utilize 32 bit accumulated data
- Exclude precipitates via image processing
- Calculate integrated Boron line profile for all image rows.
- Sum equal sized individual regions of line-profile for each alloy
- Ratio yields final Boron level = 1.8 ppm

Figure 25. RAE analysis of 12 ppm and "0"ppm samples .

32 Bit Video Data vs. RAE Data

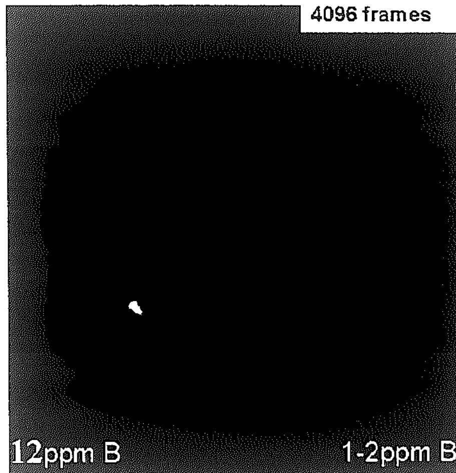

Log view of 32 bit video data

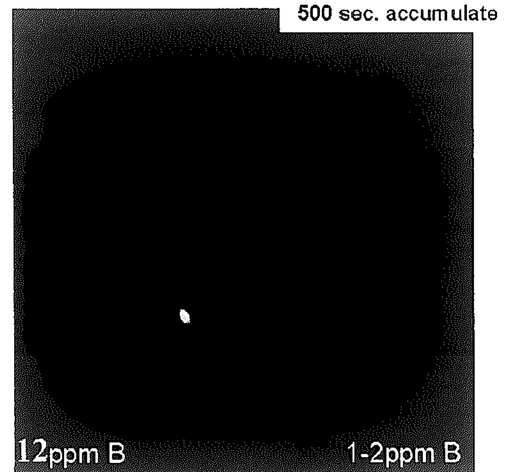

Log view of 32 bit RAE data

- Image analysis of video data yields Boron level = 1.3 ppm
- Both RAE and video results fall within range of expected value (1-2 ppm)

Figure 26. Comparison of video and RAE image data results.

32 Bit Video Data vs. RAE Data

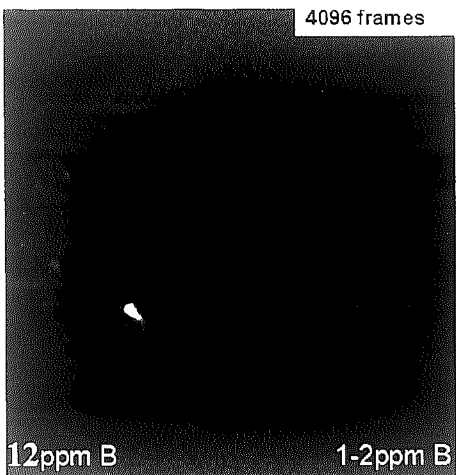

Log view of 32 bit video data

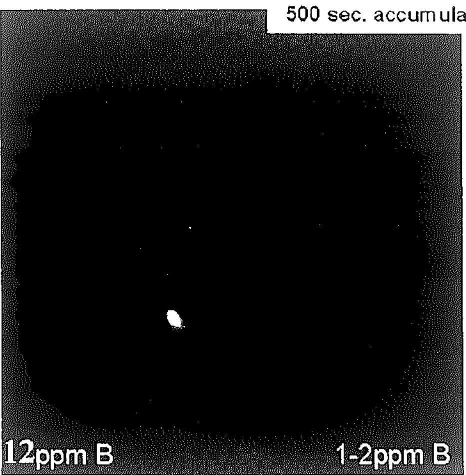

Log view of 32 bit RAE data

- Image analysis of video data yields Boron level = 1.3 ppm
- Both RAE and video results fall within range of expected value (1-2 ppm)

Figure 26. Comparison of video and RAE image data results.

Table 1. Summary of Major SIMS Quantification Schemes

Method	Reported Error Range (+/-)	Benefits	Drawbacks
Relative Sensitivity Factor ("RSF")[a]	10 - 50 %	Simple to employ on well-defined systems.	- Sample matrix must be constant and well-known. - Initial stds limit accuracy of subsequent analyses.
Ion-Implanted Internal Standard[b]	5 - 50%	Can be used for any species. Sample and standard are always analyzed together.	- Stds must be generated via ion implantation for each analysis. - Sample damage can occur during implantation.
Matrix Isotope Species Ratio ("MISR")[c]	3 - 50%	Convenient to use on homogenous samples.	- Sample heterogeneity limits accuracy. - Calibration curves need to be generated for each sample type. - Only accounts for oxide matrix effect.
CsM+ Cluster (CsM^+)[d]	10% (w/stds) 50% (w/o stds)	Relatively insensitive to most matrix effects.	- Poor sensitivity due to low signals. - Difficult on insulators.
Infinite Velocity ("IVM")[e]	10 - 300%	No standards required.	- Not useful on insulators. - High error range

[a] See ref 9.
[b] See ref 10.
[c] See ref 13.
[d] See ref 15.
[e] See ref 19.

Table 2. Outline of high-strength low alloy steel samples used in this study. (C = 0.15%, Mn = 1.50% in all alloys.)

Sample	Bulk Boron Content Added to Melt (ppm-wt)	Processing Method	Degree of Precipitation
1	12	standard	high (especially at centerline)
2	8	standard	low
3	0 (1-2 ppm due to base contamination)	standard	low
4	12	new	low

Measurement Conditions

- Employed a Cameca IMS 3f (#049) for all measurements.
- +12.5 keV (8 keV net) O_2^+ primary ions ~10μa flux (500um diam).
- +4.5 keV extraction.
- 400 - 500 μm field of view.
- Pre-sputter analysis area approximately 30 min.
- Typical boron count rate 10-100 cps.

W.A.L.

Table 3. Typical measurement conditions for imaging analysis.

Table 4. Summary of boron relative quantification results.

Expected value of boron ratio between two samples.	Average ratio (10 fields)	Standard Deviation	Standard Error of the Mean
12 ppm / 8 ppm = 1.50	1.48	0.30 (1 sigma)	1.33 %

Expected value of boron in unknown	SIMS Average (10 fields)	Standard Deviation	Standard Error of the Mean
12 ppm	11.84 (via RAE)	1.8 ppm (1 sigma)	1.33 %
1 - 2 ppm	1.8 ppm (via RAE)	N/A (only one area measured).	Not calculated due to uncertain range of expected values.
1 - 2 ppm	1.3 ppm (via Video)	N/A (only one area measured).	Not calculated due to uncertain range of expected values.

Stage of Image Conversion	Stage 0 (actual ions)		1st Stage		2nd Stage		3rd Stage
Description	Ion Image Plane with 150um field of view.	>	Channel plate	>	Fluorescent screen	>	Camera
Number of Resolution Elements (in both x & y)	750 x 750	>	1500 x 1500	>	3000 x 3000	>	6000 x 6000
Dimension of Resolution Elements	24 μm x 24 μm.	>	12 μm x12 μm, (ignoring dead space between pore channels)	>	6 μm x 6 μm	>	(depends upon sensor size and lens used) 150 μm @ 0.2 μm resolution

Table 5. Ideal spatial oversampling at each stage of image conversion.

Stage of Image Conversion	Stage 0 (actual ions)		1st Stage		2nd Stage		3rd Stage
Description	Ion Image Plane for 150um field of view.	>	Channel plate	>	Fluorescent screen	>	Camera
Number of Resolution Elements (in both x & y)	750 x 750	>	720 x 720	>	1440 x 1440	>	640 x 480
Dimension of Resolution Elements	24μm x 24μm.	>	25μm x25μm, (ignoring dead space between pore channels)	>	12.5 μm x 12.5 μm	>	(depends upon sensor size and lens used) 150um @ 5.0 um resolution

Table 6. Actual spatial sampling at each stage of image conversion for the original Cameca 3f design.

Stage of Image Conversion	Stage 0 (actual ions)		1st Stage		2nd Stage		3rd Stage
Description	Ion Image Plane for 150um field of view.	>	Channel plate	>	Fluorescent screen	>	Camera
Number of Resolution Elements (in both x & y)	750 x 750	>	1500 x 1500 (3500 available)	>	3000 x 3000 (4000 available)	>	640 x 480
Dimension of Resolution Elements	24 μm x 24 μm.	>	25μm x25μm, (ignoring dead space between pore channels)	>	12.5 μm x 12.5μm (1-3 μm crystallite size spec)	>	(depends upon sensor size and lens used) 150um @ 2.5 um resolution

Table 7(a). Spatial sampling at each stage of image conversion in improved design for this study.

Table 7(b). Calculated detected SIMS image resolution as a function of camera pixel resolution (in x & y). Assumes no error in transferring digitized data from CCD array to disk. Also assumes improved 70 lpm channel plate and 3um phosphor crystal size. 750 resolution elements intrinsic to both 150 μm & 400 μm fields. Data is plotted in figure 6 below.

Camera Resolution (pixels)	150um field of view (microns)	400um field of view (microns)
640	1.88	5
1024	1.17	3.1
2048	0.59	1.6
4096	0.29	0.77
5120	0.23	0.61
6144	0.2	0.53

Table 8. Estimation of net detector chain efficiency.				
Channel Plate	**Phosphor Screen**	**Relay Lens**	**Gen IV Intensified Camera**	**Net System Efficiency**
Conversion: ions -> electrons	*Conversion:* electrons -> photons	*No conversion:* relays photons	*Conversion:* photons -> electrons	
90 % (Some open area ratio loss) + Gain = 10^4 (electrons/ion)	100 % P20 Gain = 800 (photons/electron) w/3 keV electrons	1 % due to small solid angle	95 % Some open area ratio loss	**85.5 %** (of ions incident on channel plate)

Assumptions:

1) Conversion of ions to electrons at channel plate is primarily limited by ratio of open area to deadspace area on entry surface of channel plate. Otherwise conversion efficiency is approaching 100%.

2) High gain at exit of channel plate enables single ion events to be represented as 10^4 electrons. This burst of electrons then enters the phosphor, with a high conversion efficiency of approximately 800 photons / 1 electron.

3) Camera lens subtends a small solid angle, depending upon the geometry of the lens-to-phosphor screen optics. Estimated that only 1% of light emitted as captured and relayed to the camera.

4) GenIV intensified camera is a channel plate based device, and is thus is high gain (10^4). Efficiency limited by open area ratio as in SIMS channel plate above. Estimated efficiency at 95%. CCD efficiency is compensated by high signal levels per event from intensifier.

Major Camera Section	Individual Sub-Components	Performance Specifications	Comments
Gen IV Intensifier	- Channel Plate - Photocathode	- 18mm diameter - 7um pores - 8um c/c spacing - P43 (830 nm peak) - Response range 480nm to 920nm	- 66 lp/mm resolution - 5nsec gating possible - Higher efficiency phosphor
CCD Array	- Philips FT800N CCD	- 774 x 490 pixels - 8mm diagonal - 23% QE at 540nm - 10kx antiblooming - 100-frame on-chip integration	- High quality commercial grade chip provides reasonable cost/perf. ratio.
Peltier Cooler		- Cools down to -10C	- Minimizes CCD noise, thus improving S/N to better than 200:1 with single event sensitivity.
Camera Control	- RS-232 computer controller - Manual controller	- RS-232 protocol - Permits control of all video, cooling, & intensifier settings. - Control operations are performed in real time. - Genlock to external timer	also provides: - Gate input (5nsec) - Trigger input - Freeze frame - Internal video reference signal - Dual video outputs.

Table 9. VICCD camera components and specifications.

Vita for William A. Lamberti

Born: 10/13/61
Rockville Center, NY

Parents:
Robert A. Lamberti and Lillian A. Lamberti

B.S. Physics, 1985 St. John's University, Jamaica, NY.

Employed:

1987 - present	ExxonMobil Research and Engineering Rt. 22E Annandale, NJ 08801

END OF TITLE